Bioclogging in porous media: Model development and sensitivity to initial conditions

A. Brovelli[1], F. Malaguerra[2] and D. A. Barry

Laboratoire de technologie écologique, Institut des sciences et technologies de l'environnement, Station 2, Ecole Polytechnique Fédérale de Lausanne, CH-1015 Lausanne, Switzerland

Emails: alessandro.brovelli@epfl.ch, flm@env.dtu.dk, andrew.barry@epfl.ch

Submitted to: *Environmental Modelling and Software*

July 2, 2008

Revision #1: October 6, 2008

[1] Author to whom all correspondence should be addressed. Telephone: +41 (21) 693-5919, Facsimile: +41 (21) 693-5670
[2] Now at Department of Environmental Engineering, Technical University of Denmark, Miljøvej, Building 113, 2800 Kgs. Lingby, Denmark.

Abstract

This work presents a numerical model able to simulate the effect of biomass growth on the hydraulic properties of saturated porous media, i.e., bioclogging. A new module for an existing coupled flow and reactive-transport code-PHWAT-was implemented. Laboratory experiments were used to validate the model.. Good agreement with the experimental data was found. Model behavior was satisfactory in terms of numerical discretization errors and parameter calibration, although-grid-independent results were difficult to achieve. The new code was applied to investigate the effect of the initial conditions on clogging development. A set of simulations was conducted considering 1D and 2D flow conditions, for both uniform and heterogeneous initial biomass concentrations. The simulation results demonstrated that the rate and patterns of bioclogging development are sensitive to the initial biomass distribution. Thus, the common assumption of an initially uniform biomass distribution may not be appropriate and may introduce a significant error in the modeling results.

Keywords

PHWAT, reactive transport modeling, porosity changes, hydraulic conductivity, dispersivity, biofilm, biomass, calibration, validation

1. Introduction

Hydrodynamic and transport properties of porous media may evolve over time as a consequence of biological, chemical and physical processes. Among the most important phenomena is clogging, i.e., the reduction of porosity and permeability. Pore-clogging is a widespread process occurring in many systems, both natural and engineered. While in natural ecosystems the variation of the hydraulic properties is often moderate and subject to periodic cycles, anthropogenic disturbances may have deleterious effects and potentially change the functioning of the ecosystem itself. Clogging phenomena also play an important role in different fields related to hydro-geology and environmental engineering.

At the pore-scale, clogging is due to modifications of the geometry and effective pore radii, with an increase of the resistance to water flow, thus resulting in a decrease of both porosity and hydraulic conductivity. Several mechanisms may be responsible for the modifications of the pore-space geometry (Baveye et al., 1998; Amos and Mayer, 2006) Indeed, the most important biological process leading to clogging is the development of microbial biomass. Bacterial communities can grow in the pore space, forming continuous biofilms or isolated colonies that fill a large fraction of the pores (Baveye et al., 1998). In this work we focus primarily on bioclogging, because it often impacts on the functioning and performance of both natural and engineered ecosystems. Nevertheless, the model we describe below can be applied with few modifications to the other types of clogging.

Much experimental research has been conducted to study causes of clogging and to identify possible strategies to reduce its effects although most experiments are limited to measurements of the evolution of the bulk hydraulic conductivity with time. This type of experiment is able to provide information regarding how real, field scale systems can be managed, but gives only limited insight on the functioning of the clogging processes. In the recent years, some more detailed experiments

have also been conducted. These provide a more detailed picture of the clogging process with both 1D and 2D flow conditions (e.g., Seki et al., 1998, 2006; Islam et al., 2001; Bielefeldt et al., 2002; Thullner et al., 2002a; VanGulck and Rowe, 2004; Arnon et al., 2005; Wantanaphong et al., 2006; Ford and Harvey, 2007; Pavelic et al., 2007; Scheibe et al., 2007; Seifert and Engesgaard, 2007).

Concerning modeling, a distinction can be made between pore-scale and macro-scale models. Pore-scale simulations have often be used to investigate the effect of biomass development (as biofilms or microbial colonies) on the hydraulic conductivity, and in turn to develop or validate constitutive relationships linking porosity to permeability changes (e.g., Dupin et al., 2001; Thullner et al., 2002b; Kim and Whittle, 2006; Kapellos et al., 2007). A number of macro-scale models have been developed and used to reproduce data from laboratory experiments (e.g., Baveye and Valocchi, 1989; Taylor and Jaffé, 1990d; Tan et al., 1994; Clement et al., 1996; Kildsgaard and Engesgaard, 2001; Thullner et al., 2004) and to understand the processes governing the interactions between water flow and biomass development. The general conclusion of macro-scale modeling studies is that it is in general possible to reproduce, at least qualitatively, the development of clogging and subsequent drop of the hydraulic conductivity. Nevertheless, model applications suffer from a number of significant limitations that may hinder a model's predictive capabilities. Among the most important is the lack of robust relationship between the porosity and hydraulic conductivity (e.g., Molz et al., 1986; Baveye and Valocchi, 1989; Clement et al., 1996; Baveye et al., 1998).

Lack of information about some key properties of the physical system is another aspect that requires some attention. For example, in most previous studies a homogeneous biomass distribution was assumed. However, some works conducted considering both laboratory experiments and simulations highlighted that even relatively small heterogeneities in the initial distribution of hydraulic conductivity and bacteria can induce visible changes in the substrate consumption rates and patterns of biomass growth (Miralles-Wilhelm et al., 1997; Scholl, 2000; Magid et al., 2006; Mohamed et al., 2006). To the best of our knowledge, there is no study directly addressing the coupling between he-

terogeneity in the physical and microbiological properties and pore clogging, although it is likely that initial biomass distributions has also some effect on the rate of clogging development.

In this paper we present a modular modeling tool suitable for simulating the clogging process in 1, 2 and 3D. The model is developed at the macro-scale, and includes the effect of flow-induced shear stress on biofilms. Compared to most of the previous clogging simulators, the model we present in this work has a greater flexibility, because (i) an arbitrary reaction network can be considered and (ii) multiple components can induce pore-clogging. In the second section we apply the new simulator to two experimental datasets. These applications are used to validate the new code and to perform a sensitivity analysis to identify the critical processes and features that control the response of the system, particularly the decrease of hydraulic conductivity. An analysis of the numerical errors introduced by the additional feedback is also presented. Finally, in the fourth section we investigate the impact of initial conditions on the rate and extent of clogging.

2. Model formulation and implementation

Bioclogging is a complex phenomenon resulting from the interaction of many different processes. Biomass in porous media is present in two forms, an immobile component attached to the surface of the solid matrix or trapped by it, and the mobile component suspended in the pore-water solution. Attachment and detachment phenomena are responsible for the conversion of mobile biomass to immobile, and vice versa. In a simplified view, the detachment process is controlled by the shear stress exerted by the fluid flow on the surface of the immobile biomass, while attachment is fundamentally a deposition process (O'Melia and Ali, 1978; Reddi et al., 2000; Breadford et al., 2003; Tufenkji, 2007). Mobile biomass can be transported by pore-water flow, but can also be actively moving in response of a chemical gradient (chemotaxis) (Hornberger et al., 1992; Ford and Harvey, 2007; Tufenkji, 2007).

Other than attachment and detachment, the additional fundamental process required to properly model clogging is biomass growth and decay. This process involves both the increase of number of bacterial cells and the production of extra-cellular polysaccharides (EPS), which increases the volume of the biofilm or colonies and consequently changes the medium's porosity.

Using the macroscopic approach (e.g., Clement et al., 1997; Kildsgaard and Engesgaard, 2001), a simple relationship between the current porosity and the fraction of pore-space occupied by the biomass can be written:

$$n = n_0 - n_{bio} , \tag{1}$$

where n_0 is the porosity of the clean porous medium (i.e., without biomass), and n_{bio} is the volume fraction of biomass occupying the pore space. In porous media, biomass may be present both as single cells in the pore fluid, and as immobile aggregates and cells trapped in the pores due to their size. In this work, we assume that only the immobile fraction of the biomass contributes to the changes in pore volume. Indeed, the total volume of immobile biomass results from the sum of different constituents, such as multiple bacteria strains, EPS and macromolecules that form the structure of the biofilms (e.g., Vandevivere and Baveye 1992). As a result, the 'biological' immobile porosity is computed as a sum of the contributions of each constituent:

$$n_{bio} = \sum_{i=1}^{n} \frac{X_s^i \rho_b}{\rho_s^i} , \tag{2}$$

where X^i_s is the mass (dry weight) of the i^{th} component of the immobile biomass per unit mass of aquifer solids, ρ_b is the bulk density of the porous medium without biomass, and ρ^i_s is the density of the i^{th} component of the immobile biomass.

2.1 Processes affecting the immobile biomass

We assume that biomass growth can be modeled using a Michaelis-Menten-type equation (e.g., Bar-

ry et al., 2002), while the biomass decay is assumed to be a first-order kinetic process. We also assume that growth is only limited by the substrate (electron donor and C source) and the electron acceptor. These can be written as

$$\mu = \mu_{max} \frac{C_{ea}}{K_{ea} + C_{ea}} \frac{C_s}{K_s + C_s}, \text{ and} \tag{3}$$

$$d_r = k_d X , \tag{4}$$

where μ is the growth rate, X the biomass concentration (mobile or immobile), μ_{max} the maximum growth rate, C the concentration, K the half-saturation constant and the subscripts *ea* and *s* stand for electron acceptor and substrate, respectively. Equation (4) describes instead the biomass lysis rate d_r, with k_d being a first-order decay constant.

The modeling assumptions used here are commonly found in biomass simulations, including all the existing bioclogging models (Clement et al., 1996; Kildsgaard and Engesgaard, 2001; Thullner et al., 2004). As will be made clear later, however, one of the strengths of our approach is that such assumptions can easily be modified, and potentially any equation can be used to describe the growth/decay process.

Biomass growth is also self-limited, in that it reduces the available pore space and reduces the nutrient and carbon source fluxes (e.g., Kindred and Celia, 1989; Prommer and Barry, 2005). A mathematical expression that accounts for these two phenomena was proposed by Zysset et al. (1994), and has already been used in bioclogging models (Kildsgaard and Engesgaard, 2001):

$$I_{bio} = \frac{X^{max} - \left(X_s + X_a\right)}{X^{max}}, \tag{5}$$

where X^{max} is the maximum possible biomass content of the porous medium per mass of solids, X_a and X_s the current amounts of mobile and immobile biomass, respectively. As discussed by

Kildsgaard and Engesgaard (2001), an upper bound for I_{bio} is given can be computed considering the volume of pore space in the clean porous medium, i.e., its porosity. In practice, however, this value is always smaller than its upper bound because as biomass grows nutrient transport becomes progressively a diffusion-controlled process.

Attachment and detachment processes are instead less well understood and only a small number of theoretical studies have been carried out to elucidate the effect of various chemical and physical properties on both the porous medium and the pore-water solution on their rates. Most of the available equations contain inconsistencies and weaknesses that limit model applicability and robustness (Tufenkji, 2007). The more often used equations are based on colloid filtration theory, which has probably only limited applicability to bacteria motility (Rittmann, 1982; Harvey and Garabedian, 1991; Reddi et al., 2000; Tufenkji, 2007). Recently, a number of experimental and theoretical investigations have been carried out, but there still is a lack of reliable, closed-form constitutive relationships (e.g., Breadford et al., 2003; Gargiulo et al., 2007; Jiang et al., 2007; Scheibe et al., 2007). For these reasons, and following previous works (Clement et al., 1996; Kildsgaard and Engesgaard, 2001; Thullner et al., 2004; Tufenkji, 2007), we adopted the classical equations from deep-bed filtration.

The attachment coefficient is computed as (Harvey and Garabedian, 1991; Scheibe et al., 2007):

$$k_{att} = \frac{3(1-n)v_p\eta}{2d_g}, \tag{6}$$

where v_p is the pore velocity, n the porosity, d_g is a characteristic grain diameter and η the collector efficiency, a parameter representing the frequency of collisions between mobile bacteria and grain surfaces. Some relationships have been proposed to compute the collector efficiency (Tien et al., 1979; Scheibe et al., 2007). Such equations however contain some parameters that are difficult to measure or estimate. For this reason, we considered the collector efficiency as an empirical parame-

ter and estimated it during model calibration.

The sensitivity and importance of shear detachment has been debated in the literature, and no unique approach can be identified. According to Thullner et al. (2004), shear detachment can be safely neglected, at least when the flow field is 2D, while Kildsgaard and Engesgaard (2001), also considering a 2D flow field, found good agreement using a simplified law independent from flow velocity. We decided instead to consider the dependency of the detachment rate on the flow velocity, and to implement the semi-empirical equation proposed by Rittmann (1982):

$$k_{det} = c_d \left[\frac{\gamma v_p (1-n)^3}{d_p^2 n^3 M} \right]^{0.58} , \quad (7)$$

where k_{det} is the detachment rate, $\gamma$is the viscosity of water, d_p is the characteristic grain diameter, M the specific surface area and c_d an empirical parameter. By calibrating the model on experimental datasets, Rittmann (1982) proposed a value of 2.29×10^{-6} for c_d. As this value is dependent on the experimental circumstances, it was calibrated in the applications presented below.

Upon combining the different processes, the following coupled ODEs describing biomass variation in time are obtained:

$$\frac{\partial X_s}{\partial t} = \mu_s I_{bio} X_s - k_d X_s - k_{det} X_s + k_{att} X_a \text{ and} \quad (8)$$

$$\frac{\partial X_a}{\partial t} = \mu_a I_{bio} X_a - k_d X_a + k_{det} X_s - k_{att} X_a , \quad (9)$$

where the subscripts *s* and *a* refer to the immobile and mobile biomass, respectively. As has been assumed by others (Taylor and Jaffé, 1990b; Kildsgaard and Engesgaard, 2001; Clement et al., 1996), we do not consider separately living cells and EPS. Biofilms are composed of nearly 95% water, and it is consequently reasonable to assume that their density is equal to that of water. Since

187 the mass fraction of soil grains and water phase remains constant over time, we can express solid
188 biomass in terms of pore-fluid concentration instead of concentration per unit mass of soil.

189 ## *2.2 Hydraulic conductivity changes*

190 The relationship linking permeability to porosity changes is non-trivial to define. Permeability de-
191 pends on a large number of micro-structural and geometrical properties of the porous structure, such
192 as pore size distribution, pore shape, pore connectivity and tortuosity. All these properties cannot be
193 directly deduced from the changes in the porosity, and depend primarily on the biomass configura-
194 tion and distribution at the pore level. A number of constitutive relationships have been proposed,
195 such as the well-known Kozeny-Carman formula, but none is generally applicable (Zheng and Ben-
196 nett, 2002). A sub-set of these relationships has been developed to account for the properties of the
197 biomass aggregates (Vandevivere et al., 1995; Baveye et al., 1998). Among the most well known
198 are the model of Clement et al. (1996), the colonies and the biofilm models (Thullner et al., 2002b).
199 These relationships rely on a simplified description of both the porous medium and biomass, and
200 have been found to be suitable to reproduce the clogging patterns observed in several experiments.
201 The main difference between these three functions is in the geometry of the immobile biomass, and
202 the fraction of pore space that is occupied initially.

203 It has been observed that an exponential relationship between porosity and hydraulic conductivity is
204 often found in experimental data (Sahimi, 1995; Clement et al., 1996). Several authors (Ives and
205 Pienvichitr, 1965; Okubo and Matsumoto, 1979; Knapp et al., 1988; Taylor and Jaffé, 1990b) pro-
206 posed consequently the relationship:

207 $$K_{rel}\left(n_{rel}\right) = n_{rel}^{p}\ ,\ p > 0 \qquad (10)$$

208 where K_{rel} and n_{rel} are the relative hydraulic conductivity and porosity (defined respectively as n/n_0
209 and K/K_0). Here and in the following, K denotes the hydraulic conductivity, and the subscript 0 in-
210 dicates the hydraulic conductivity of the clean porous medium. The exponent p is a parameter that

211 depends on the micro-geometrical properties of the porous medium and on the morphology of the
212 biomass. We note that Equation (10) is analogous to the unsaturated hydraulic conductivity for wa-
213 ter flow in a porous medium (references), where n_{rel} is replaced by the normalized moisture content.
214 There, the physical basis of the rapid decline in relative conductivity with moisture content is that
215 the larger pores drain most readily due to capillarity. On that basis, whatever the derivation of Equa-
216 tion (10), its use in bioclogging models is entirely consistent with the notion that the biomass clogs
217 the larger pores in preference to smaller pores. Clement et al. (1996) developed a relationship
218 equivalent to Equation (10) considering the pore-size distribution and a relationship between rela-
219 tive water saturation and pressure head. An explicit dependence between the exponent p and the
220 pore-radius distribution was obtained. It was found that for typical sandy materials, it is appropriate
221 to take p = 19/6. Since Clement's model was developed considering the analogy with drainage,
222 where larger pores are initially drained, the underlying assumption of this constitutive equation is
223 that the larger pores fill first with biomass.

224 The other two models we consider were not derived using analytical descriptions of the porous
225 structure, but on pore-network simulations that were carried out considering different conditions,
226 with the results fitted to closed-form relationships. The colonies model (Thullner et al., 2002b) as-
227 sumes that the total biomass in the medium is split into different entities and that bacterial growth
228 occurs in the smallest pores first. This model is thus a contrast to the Clement model, in which the
229 larger pores are clogged first. The colonies model is expressed as:

230 $$K_{rel}\left(n_{rel}\right) = a\left(\frac{n_{rel} - n_{rel}^{0}}{1 - n_{rel}^{0}}\right)^{3} + \left(1 - a\right)\left(\frac{n_{rel} - n_{rel}^{0}}{1 - n_{rel}^{0}}\right)^{2}, \quad (11)$$

231 where a and n^{0}_{rel} are adjustable parameters, with 1- n_{rel}^{0} being interpreted as the relative volume of
232 biomass needed to get the maximum reduction of hydraulic conductivity, i.e., the hydraulic conduc-
233 tivity goes to 0 as the relative porosity n_{rel} approaches n_{rel}^{0}. Model fitting on experimental data

234 shows reasonably good agreement (Thullner et al., 2004). The parameter n_{rel}^{0} was found in most of
235 the cases in the range 0.4-0.9 while *a* was found between -1 and -1.9.

236 A third concept to pore clogging is the biofilm model of Thullner et al., (2002b), which assumes a
237 single, connected layer of biomass covering the wall of each pore. As a consequence of biofilm de-
238 velopment, the pore-radius is reduced and therefore also water flow and solute transport is mod-
239 ified. In the pore-network simulations used to derive this model, a growth-limiting nutrient was
240 considered. The final relationship is:

241 $$K_{rel}\left(n_{rel}\right)=\left[\left(\frac{n_{rel}-n_{rel}^{0}}{1-n_{rel}^{0}}\right)^{b}+K_{min}\right]\frac{1}{1+K_{min}}, \qquad (12)$$

242 where K_{min} is the lower limit of hydraulic conductivity, i.e., the value of hydraulic conductivity
243 when n_{rel} approaches n_{rel}^{0}, similar to the colonies model. Applying the biofilm model to experimen-
244 tal data (Thullner et al., 2004) resulted in a good fit, with the parameter n_{rel}^{0} in the range 0.2-0.4 and
245 6×10^{-3}-10^{-2} for K_{min}.

246 ## *2.3 Model implementation*

247 A new clogging module was implemented for the numerical model PHWAT (Mao et al., 2006),
248 which evolved from PHT3D (Prommer et al., 1999a,b, 2000, 2003). PHWAT is a computer code for
249 3D reactive transport in variable-density saturated flow. PHWAT was developed coupling SEAWAT
250 (Guo and Langevin, 2002) with the aqueous chemistry model PHREEQC (Parkhurst and Appelo,
251 1999). The variable-density model SEAWAT is also a coupling between two other software pack-
252 ages, MODFLOW-88 for water flow (McDonald and Harbaugh, 1988) and MT3DMS for solute
253 transport (Zheng and Wang, 1999). A sequential non-iterative operator splitting algorithm was used
254 to couple solute transport and biochemical reactions. The resulting model has a modular structure.
255 Therefore, additional capabilities can be implemented as separate modules The bioclogging module

consists of three main subroutines. The first subroutine computes the coefficient required during the reaction step, namely the attachment, detachment and activity coefficients (Equations 5-7). This is done computing the Darcy flux and pore-water velocity from the current hydraulic head, conductivity and porosity. The coefficients are subsequently used during the reaction step to compute the mobile and immobile biomass concentrations (Equations 8 and 9). The second subroutine updates the porosity, comparing the immobile biomass concentration at present and previous time step. The new value for the mobile porosity is computed from Equations 1 and 2. Next, the third subroutine updates the hydraulic conductivity using one of the constitutive equations implemented (Equations 10 to 12). As already discussed, these equations were selected because previous works showed they provide a good fit of experimental data for bioclogging studies. Nevertheless, additional constitutive equations can easily be incorporated in order to extend the model to account for clogging phenomena originating from different processes and with different behavior, e.g., due to mineral phase precipitation/dissolution, or entrapment of gas bubbles.

During model testing we found the embedded PHREEQC reaction module to be very slow sometimes for calculation of reaction kinetics. For this reason, an alternative module was developed. This alternative biogeochemical module implements the standard $4^{th}/5^{th}$ order Runge-Kutta solver and can save up to 50% of the CPU time compared with PHREEQC.

3. Model validation with experimental data

As already discussed in the introduction, some experimental results are available in the literature. These can be used to test and validate the numerical model. Design and implementation of such laboratory experiments is difficult, since potentially the hydraulic properties change rapidly in space, and a high resolution sampling regime would be required to capture well the evolution in space and time.

In order to validate the numerical model presented in the previous section, we selected two laboratory experiments conducted using different setups and different approaches to monitor the evolution of biomass development in the porous medium. This choice allows us to test the model under different conditions, and to assess the model sensitivity to different parameters.

3.1 Column experiment with bioclogging

The numerical model was first tested against the 1D laboratory experiment of Taylor and Jaffé (1990a). The setup consists of a plastic column filled with sand. Bacteria and organic carbon were removed by incinerating the porous medium before packing. Next the column was flushed for a period of four hydraulic retention times to seed it with a solution containing a mineral growth medium, bacteria and methanol as the carbon source. Table 1 summarizes the main properties of the experimental setup and of the porous medium.

TABLE 1 NEAR HERE

Two experiments were carried out simultaneously using different substrate concentrations and flow rates, but detailed information on the evolution of the hydraulic head at different heights are available only for one of them. For this reason, in the rest of the work we only consider data from experiment #1 of Taylor and Jaffé (1990a). The experiments were run continuously pumping a solution containing the mineral growth medium and methanol, but without biomass. The concentration of methanol was selected to prevent complete oxygen depletion inside the column, based on estimated consumption rates. This is a significant advantage for numerical modeling, since assuming that oxygen is not a limiting factor permits some simplification of the reaction network, thus reducing the number of parameters in the model. Flow rates were instead chosen to produce Darcy velocities similar to those observed near injection wells, which are higher than those occurring in aquifer. As will be discussed later, this has some negative consequences for modeling.

Hydraulic heads and substrate concentrations were monitored every one to four days during the first phase of the experiment (106 d), while the sampling frequency was reduced during the second part. The hydraulic conductivity was computed via Darcy's law from the measured hydraulic head between two consecutive measurement ports. The computed hydraulic conductivity is thus an average value reflecting the distribution of this parameter between two sampling ports.

3.1.1 Model setup

The column used during the laboratory experiments was discretized with a 1D grid of 52, 0.01-m cells. Numerical experiments were carried out to ensure grid-independent results. Simulation results were also compared to those obtained with an equivalent 2D domain, with excellent agreement. All the initial hydrodynamic properties are known from the experiment, except for the longitudinal dispersivity (α_L), which was set to 10^{-2} m according to values for similar sands at the same length scale (Zheng and Bennett, 2002). The molecular diffusion coefficient (d) was instead assumed negligible compared to the hydrodynamic dispersion and was consequently set to zero.

Following the experimental setup, a flow boundary condition was used at the inlet both for water and solutes, while a fixed hydraulic head was set at the exit of the simulated column. The value of the hydraulic head was set high enough so that the whole column remains fully saturated during the simulation period. As for the initial conditions, the concentrations of all the components were set to zero, except for the immobile biomass. No information is available about the concentration of this component or its spatial distribution and density within the column. For this test case, we set a homogeneous small concentration throughout the modeled domain (10^{-6} mol l^{-1}). Indeed, we found the choice of the initial biomass distribution may have a significant impact on the development of biomass and thus on the patterns of clogging. For this reason, a detailed sensitivity analysis was carried out and is described in the fourth section of this work.

As already pointed out, the flow rate adopted during the experiment is large, resulting in average

pore velocity at the beginning of the experiment of about 5.5 m d^{-1}, increasing up to about 38 m d^{-1} as the pores become increasingly clogged (here we assume a residual porosity of 5%). This has some consequences for the numerical modeling since to control the split-operator error associated with the coupling of the transport and reaction equations a refined time step is needed. Numerical experiments were conducted to choose an appropriate time step. A summary of the results and some discussion is presented in Section 3.1.4, but here we anticipate that we found the best results using a constant time step of about 45 s.

The Total Variation Diminishing (TVD) method was used to solve the transport equation. It is a high-order finite-difference (Eulerian) scheme, with the advantages of being mass conservative, oscillation-free and with small numerical dispersion (Zheng and Bennett, 2002).

According to Taylor and Jaffé (1990a), methanol concentrations were selected to avoid oxygen being completely depleted. Consequently, the Monod-type equation introduced above was used (Equation 3) to model substrate consumption, but the electron-acceptor limitation was removed.

3.1.2 Model calibration

Various parameters are unknown and were adjusted to fit the experimental data. Model calibration is complex because the different biological and physical processes are highly non-linear. Depending on the porosity-hydraulic conductivity relationship used, the number of parameters that it is possible to tune is between 8 and 11. An initial sensitivity analysis involving sequential parameter variation identified three key variables, viz., the maximum growth rate for biomass, and the coefficients controlling the attachment and detachment rates. In order to reduce the complexity of the inverse problem, only these parameters were initially optimized.

Automated model calibration was performed using PEST (Doherty, 1998), a general-purpose program for gradient-based calibration and optimization. The main limitation of the method is that, while it is very efficient for linear and quasi-linear models, it is easily trapped in local minima,

which is the case for reactive transport models. However, the same algorithm implemented in PEST has been often used to calibrate reactive transport models, and proved effective in a number of cases (Dai and Samper, 2004; Shawn Matott and Rabideau, 2008). In order to partially overcome these difficulties, we coupled the model calibration performed with PEST with a Latin-Hypercube multi-restart technique (e.g., Bajracharya and Barry, 1995). The parameter space was subdivided into regular intervals (the range of each parameter was divided into three sub-intervals), and within each interval a value was randomly selected and used as the initial guess for the Levenberg-Marquardt algorithm. Because of the computational cost, this approach works well only when the number of parameters to be calibrated is small.

FIGURE 1 NEAR HERE

3.1.3 Results and comparison with experimental data

Only the experimental data after 14, 28 and 42 d since the beginning of the experiment were used to validate the numerical model, although the experiment was run for 283 d. We decided not to consider the experimental results at later times because the pattern of the permeability decrease shows a radically different behavior. It is likely that at later times the main clogging mechanism is not directly related to further biomass growth, because all the substrate is consumed near the inlet to maintain the existing biomass. As suggested by other works (Seki et al., 1998; Bielefeldt et al. 2002), possible alternative causes for the observed hydraulic conductivity reduction are the filtration of colloids and fine particles suspended in the pore fluid (e.g., dead cells and detached polymers) or the presence of gas bubbles, factors that were not included in the model. This difference was reflected in the difficulty in the model's ability to fit the data, e.g., unreasonably large parameter changes. As described below, the early-time model calibration did not make reasonable predictions for data collected at later times.

The model parameters were calibrated on the experimental data measured at 14 and 28 d, while ex-

perimental data at 42 d were used to verify to what extent the model can be used as a predictive tool. Experimental data and the best simulations obtained using PEST are compared in Figure 1. Overall, model results show a reasonably good agreement with the experiment and, among the published modeling results that are compared to this experiment (e.g., Taylor and Jaffé, 1990c; Ham et al., 2007), this model shows (at least visually) the best agreement. Indeed, while the fit is excellent at 28 d, the predicted permeability reduction significantly underestimates the measured value near the column inlet at 14 d. It is possible to improve the fit by giving more weight to the early results than to those at 28 d, but this gives a significant decrease in the quality of the fit at later times. Moreover, it should be noted that, while the parameter set we are using is that providing the best fit (i.e., the lowest value of the weighted residuals), a relatively good fit can be obtained with significantly different values for the three parameters we calibrate. This is possibly due to the presence of local minima, which limits the validity of the model as an explanatory and forecasting tool. This is a common challenge in modeling biogeochemical processes, and in the case of bioclogging it is further evident because of the additional processes considered and the feedback of biological reactions on water flow and solute transport.

Simulated results at 42 d, not used during model calibration, show good agreement up to 0.15 m from the inlet. Instead, while in the experiment there is a transition zone where the relative conductivity gradually changes from about 10^{-3} to unity over a distance of 0.2 m, the same transition in the simulated results is sharper and requires only 0.15 m. This happens at later times, with an even more pronounced difference. While in the simulation the clogging front moves gradually towards the outlet without a significant change in the shape and slope, in the experiment the front become broader and more stretched.

The substrate distribution within the column was measured 14 d after starting the experiment. Figure 2 shows the experimental and simulated data. The modeling results correctly reproduce the observed sharp decline of concentration near the inlet. Only the measured value of methanol near the

399 inlet shows a significant difference with the simulation. However, the observed concentration is
400 very close to the initial concentration (about 7 mg l^{-1}). It is likely that the measurements are strongly
401 affected by the influent solution composition. The simulated value is instead an average of the con-
402 centration in the first cell, where the concentration of biomass is higher, and thus the transformation
403 rate for methanol is also high.

404 **FIGURE 2 NEAR HERE**

405 ### 3.1.4 Model accuracy

406 As already mentioned, incorporating the additional feedback due to clogging in a numerical simula-
407 tion may require more stringent constraints than normal on the grid and time discretization to main-
408 tain the accuracy of the numerical results. For this reason, we carefully investigated the effect of
409 discretization using a set of numerical experiments that considered different grid and time step siz-
410 es. The effect of both grid refinement and dispersivity on the accuracy of the results was investi-
411 gated by means of the grid Péclet and Courant numbers. The Péclet number *Pe* is:

412 $$Pe = \frac{v\Delta L}{D} = \frac{v\Delta L}{d + v\alpha_L} \approx \frac{\Delta L}{\alpha_L}, \qquad (12)$$

413 where v is the pore water velocity, D the hydrodynamic dispersion coefficient and ΔL the grid spac-
414 ing. If Eulerian schemes are used to solve the advective term of the transport equation, a common
415 constraint for this criterion is $Pe < 5$ (Zheng and Bennett, 2002). Indeed, for the current simulations
416 *Pe* not only affects stability and accuracy of the numerical scheme, but also the correct development
417 of the porosity and hydraulic conductivity changes. Since within each cell the concentration of each
418 component is constant, an excessively coarse grid spacing is not able to capture the correct develop-
419 ment of the clogging front, and in turn the water flow is not updated correctly. This is similar to
420 what is observed in variable density flow simulations, where a coarse grid does not properly capture

instabilities at the interface between fresh and dense water. In such cases, it is appropriate to use a more stringent constraint to achieve a better accuracy, e.g., $Pe \leq 2$ (Zheng and Bennett, 2002; Brovelli et al., 2007).

TABLE 2 NEAR HERE

FIGURE 3 NEAR HERE

FIGURE 4 NEAR HERE

Table 2 summarizes the four test cases considered, while Figures 3 and 4 compare, respectively, the porosity and hydraulic conductivity profiles for the same four cases. The figures are divided in two panels with results obtained setting the longitudinal dispersivity to the same value. The left panel of both Figures 2 and 3 shows that even $Pe = 2$ may not be appropriate to capture correctly the clogging front. Comparing the results of the four simulations in Figures 3 and 4, it is clear that the difference is significantly larger in the hydraulic conductivity profile than in the porosity profile. The reason for this different behavior is related to the exponential relationship between the two quantities. The relative error was also computed, both for porosity and hydraulic conductivity (Figure 5). The larger error is found in the area near the inlet, with values as high as 45% for Cases A-B, and 8% for Cases C-D. This is not surprising as this is the zone with the larger biomass growth and higher flow velocity. Moreover, for Cases A-B a significant error is visible in the area around the clogging front, indicating that $Pe = 2$ is not suitable to properly capture the patterns of clogging.

Cases C and D show a much better agreement, but some differences are still visible. The error for the porosity profile is always below 3%, while the error on the conductivity profile is larger but always below 10%. Again, the more critical areas are near the inlet and adjacent to the clogging front. This indicates that resolution-independent results are extremely difficult to achieve, and when the transport is dominated by advection this effect is more pronounced. Following this analysis, we take

444 Pe = 1, as it provides a good balance between accuracy of the solution and CPU time needed.

445 **FIGURE 5 NEAR HERE**

446 **FIGURE 6 NEAR HERE**

447 **FIGURE 7 NEAR HERE**

448 Apart from the grid spacing, numerical results are greatly affected by the time stepping. Two differ-
449 ent errors can potentially be introduced (i) an error associated with the solution of the transport equ-
450 ation and (ii) the operator splitting error (OSE), related to the sequential solution of water flow, so-
451 lute transport and biogeochemical processes. The first error is automatically controlled by the trans-
452 port module of PHWAT, which selects the more appropriate time step size on order to obtain an ac-
453 curate solution (Zheng and Wang, 1999). Instead, a time step size suitable to minimize the OSE
454 must be decided case-by-case. For this reason, we conducted a set of numerical experiments using
455 different time steps for the coupling between transport and biochemical reactions. We also used
456 these tests to ascertain whether the additional processes and non-linearities introduced when ac-
457 counting for clogging require a reduced time step. Simulated biomass profiles obtained when clog-
458 ging is accounted for were compared with the results for the same model setup but with the clog-
459 ging module disabled. Results are compared using the Courant number (Cr) (Zheng and Bennett,
460 2002):

461 $$Cr = \frac{v\Delta t}{\Delta L} \tag{13}$$

462 where Δt is the time step size. In the simulations with clogging, due to the constant flux boundary
463 condition at the surface, the average pore velocity v increases as the porosity decreases, and thus the
464 Courant number varies in space and time. In order to compare results with the simulations without
465 clogging, Cr was computed using the initial (constant) porosity.

The immobile biomass profiles for three different *Cr* values are shown in Figure 6. In the left panel are plotted the results of the simulations with clogging, while on the right panel the results with constant porosity and conductivity. Comparing the two pictures it is clear that the effect of the OSE is a smearing of the immobile biomass concentration peak in the first cells, behavior that is consistent with analyses that show that the splitting can introduce numerical dispersion (Barry et al., 1997). It is also evident that the amplitude of the peak is smaller when the clogging module is active. This is likely to be due to the increase in flow velocity as a consequence of the porosity decrease, which in turn increases the shear stress on the biofilm. In the model, this phenomenon results in a larger detachment coefficient. The OSE of the simulations with $Cr = 0.4$ and $Cr = 2$ relative to the case with $Cr = 0.1$ was computed and is reported in Figure 7. Surprisingly, the error is smaller in the simulations with clogging than in those were the porosity is kept constant. This can be again explained considering the increase of detachment rate when the porosity decreases. The main biochemical reaction considered in the model is the consumption of substrate and subsequent biomass growth. The process of shear detachment reduces instead the biomass growth, which is equivalent to a reduction of the biomass growth rate and thus of the OSE. The same behavior was observed with different growth and water flow rates. According to these results, the feedback of the biological growth on solute transport does not require a smaller time step than simulations conducted without considering clogging.

3.2 2D clogging experiment

3.2.1 Experimental setup

Kildsgaard and Engesgaard (2002) reported a laboratory experiment conducted to investigate bioclogging under 2D flow conditions. The experimental system consisted of a rectangular thin box filled with sand. The dimensions and main properties of the device and experiment are reported in Table 3. The sand was incinerated prior to packing the porous medium. Next, a strip of sand near

490 the center of the box was inoculated with biomass (Figure 8). The bacterial community was taken
491 from the effluent of a wastewater treatment plant (after the nitrification step). Background water
492 flow (degassed tap water) was applied at a constant rate. A solution of acetate ($CH_3COONa \cdot 3H_20$)
493 as electron donor and nitrate (KNO_3) as electron acceptor was prepared using untreated tap water
494 and injected in the chamber through a needle placed in the center of the device, upstream to the in-
495 oculated strip.

496 **TABLE 3 NEAR HERE**

497 **FIGURE 10 NEAR HERE**

498 Biomass growth and subsequent changes of the flow field were visualized conducting tracer experi-
499 ments at regular intervals (1 to 3 d). Brilliant Blue tracer was used, which is nontoxic and only
500 slowly biodegraded. It is however sorbed to the sand surface, but the equilibrium partitioning con-
501 stant is known and was used in the model. The time and space evolution of the plume was recorded
502 taking camera snapshots and the actual concentration of colorant was recovered using image-
503 processing techniques. Further details can be found in Kildsgaard and Engesgaard (2002).

504 ### 3.2.2 Numerical model

505 A 2D regular grid was used to simulate the experimental setup of Kildsgaard and Engesgaard
506 (2002). The optimal grid spacing was of 5×10^{-3} m, resulting in finite difference grid of 2640 nodes,
507 while the time step was 10^{-3} d. With this discretization the simulation of 20 d required about 1.5 d of
508 CPU time on an Intel Xeon 2.33 GHz machine. Flux boundary conditions were used along the top
509 and bottom (Figure 8) of the domain (other sides set to zero flux), as well as to simulate the injec-
510 tion needle. A small initial concentration of immobile biomass was used to reproduce the sand strip
511 inoculated with bacteria. The biomass concentration in the inlet water was assumed negligible and
512 set to zero. Following the experiment, we simulated tracer experiments for comparison with the la-
513 boratory data.

A numerical model reproducing the experiment is available (Kildsgaard and Engesgaard, 2001). Therefore, instead of calibrating the missing parameters, we used the same values as Kildsgaard and Engesgaard (2001). This provides a way to verify the computer code, as well as reducing the computational burden by removing the calibration exercise. The major difference between our description of the clogging process and the previous implementation is in the attachment and detachment coefficients. Whereas the two coefficients are constant in Kildsgaard and Engesgaard (2001), in our model they are dependent on the flow velocity. To be able to compare our simulated results with the measured tracer concentrations using the published parameter set, they were initially fixed. Following this, the dependency on flow velocity was introduced to investigate the effect and sensitivity of these two parameters. A few parameters were still missing, and were taken from Clement et al. (1997).

FIGURE 9 NEAR HERE

FIGURE 10 NEAR HERE

3.2.3 Results and comparison with experimental data

To able to compare the results of our simulations with those of Kildsgaard and Engesgaard (2001), the numerical model was first run using the porosity-hydraulic conductivity constitutive relationship proposed by Clement et al. (1996), with the detachment rate independent of the flow velocity. Figure 9 shows the evolution of the mobile and immobile biomass concentration as a function of time with this model setup. As soon as the feed solution reaches the zone where the sand is seeded with bacteria, the immobile biomass starts growing, in turn reducing the porosity and hydraulic conductivity within a strip parallel to the flow direction. The aqueous biomass concentration starts increasing as well, being related to the concentration of immobile biomass. While at early time (5-10 d) the shape of the suspended biomass plume is similar to a strip and has constant width, when the clogging becomes more intense (17-25 d) the upstream part of the plume is larger and rounded, while

538 the part close to the outlet is again a strip of constant with. This is related to the development of a
539 more complex flow field around the clogged area, with most of the water bypassing the area with
540 lower hydraulic conductivity (Figure 10). The branched shape of the immobile biomass is also re-
541 lated to the increased complexity of the flow field. The carbon source and nutrients injected with
542 water do not penetrate into the clogged zone, but bypass it flowing along the edges. Only in this
543 area can biomass grow. Due to the lack of nutrients, within the clogged zone, the growth rate de-
544 creases to zero and decay becomes predominant, thus leading to a decrease in biomass and conse-
545 quently to an increase of the hydraulic conductivity.

546 The results of the simulated tracer experiment conducted with the numerical model were compared
547 with the laboratory results. The comparison is reported in Figure 11 for results at 10 and 17 d. To-
548 gether with the simulated tracer concentrations obtained using the Clement model; here also the re-
549 sults obtained using the biofilm and colonies model are shown. Figure 12 reports instead the evolu-
550 tion of the hydraulic conductivity over time, as predicted by the three relationships. The simulated
551 results represent reasonably well the experiment, with no parameter adjustments. The two-branch
552 shape of the plume is correctly reproduced. However, while the Clement and biofilm models better
553 reproduce the experimental data at 10 d, the plume obtained with the colonies model is a closer
554 match to the experiment at 17 d. The Clement and biofilm models show a very similar pattern of
555 hydraulic conductivity change. Indeed, a quantitative comparison of the results obtained with the
556 two models show that the biofilm model leads to less clogging than Clement's. The reason for this
557 is the larger hydraulic conductivity decrease at small porosity changes in the Clement model.

558 **FIGURE 11 NEAR HERE**

559 **FIGURE 12 NEAR HERE**

560 Both our simulations and those of Kildsgaard and Engesgaard (2001) show some discrepancies with
561 the experimental (Figure 11). First, the downstream concentration gradient near the front of the

562 plume is sharper in the experiment than in the simulations. This is surprising because other investi-
563 gations have reported that clogging leads to a significant increase in dispersion coefficients (Taylor
564 and Jaffé, 1990c; Bielefeldt et al., 2002; Seifert and Engesgaard, 2007). There is no clear explana-
565 tion for this difference. However, two possible sources of error can be identified (i) the image
566 processing technique used to measure the concentration possibly does not resolve well the gradient,
567 and (ii) the tracer sorption on sand or to the transparent top of the sandbox may hide the devel-
568 opment of a concentration gradient. The other difference between experiment and simulation is the
569 development of a broader plume in the upstream clogged area. The reason for such a difference may
570 be found in the partial clogging of the area surrounding the injection nozzle, due for example to
571 biomass growth, formation of gas bubbles or calcite precipitation (Kildsgaard and Engesgaard,
572 2001). The clogging of this area decreases the hydraulic conductivity and therefore leads to a more
573 dispersed flow. Kildsgaard and Engesgaard (2001) partially reproduced the observed behavior as-
574 suming that a small amount of biomass was present in the tap water used to prepare the feed solu-
575 tion, thus inducing some partial clogging of the medium near the inlet. We did not consider this
576 process in our model because it seems to produce excessive lateral spreading of the tracer plume at
577 later times (Kildsgaard and Engesgaard, 2001, Figure 8), while it has little if any impact before 15
578 d. A possible reason is that other clogging processes (biogenic gas production and mineral phase
579 precipitation) are more important and cannot be correctly reproduced as bioclogging.

580 Next, we conducted some numerical experiments to investigate the sensitivity of clogging to the
581 detachment rate. We found that, as soon as the flow rate increases, most of the biomass is detached
582 and clogging does not take place. Therefore, it seems that only a very weak dependence of the de-
583 tachment rate is required. It is likely that different parameters (maximum growth rate and attach-
584 ment rate) would be required to match the experimental dataset when the flow-dependent detach-
585 ment rate is activated. We did not try to find such a parameter set because the system is already suf-
586 ficiently parameterized. Considering one more parameter only increases the flexibility of the model

587 but in this case does not improve the insights one can gain from model-based analysis of the experi-
588 mental data.

589 *3.3 Discussion of model application to experiment data*

590 Modeling results and experimental data show satisfactory qualitative agreement both for the 1D
591 case of Taylor and Jaffé (1990a) and for the 2D experiment of Kildsgaard and Engesgaard (2002).
592 Although most of the features observed in the experiments are reproduced in the simulations with a
593 good degree of accuracy, open issues remain that require further investigation and improvements of
594 both experimental systems and modeling.

595 As noted earlier, the link between porosity and hydraulic conductivity changes is not yet well un-
596 derstood and still lacks a robust constitutive relationship. Our simulations show that the Clement
597 and biofilm models seem more suitable for moderate clogging, while the colonies model gives in-
598 stead more realistic results when clogging is pronounced. This finding accords with the conclusions
599 of Thullner et al. (2002b) and Seifert (2005), who noted that it is likely that the biomass morphol-
600 ogy changes as clogging becomes more severe. The three models make different assumptions re-
601 garding the fraction of pore-space occupied by the bacteria. In particular, the colonies model as-
602 sumes that small pores are blocked first. Our results seem to indicate that this assumption is not va-
603 lid for early times as the simulations conducted with this constitutive relationship cannot match the
604 experimental results. However, as will be discussed below, the initial biomass distribution is an im-
605 portant factor in clogging development, making it difficult to isolate the different effects of the
606 clogging models used.

607 The detachment coefficient shows a different sensitivity depending on the flow conditions. While
608 for the 1D column experiment of Taylor and Jaffé (1990a) the modeling results are strongly affected
609 by this parameter, bioclogging in a 2D flow field is slightly sensitive to the flow-dependent detach-
610 ment coefficient. The same conclusion was also reported in other works (Kildsgaard and Enges-

gaard, 2001; Thullner et al., 2004). While in the 1D case the clogging is rather uniform in a given cross-section of the column, leading to a uniform increase of the pore-velocity, in the 2D flow field alternative, non-clogged flow paths remain. Consequently, the increase of pore velocity is moderate, and biomass is less influenced by shear stress.

As for many reactive transport models, significant difficulties were found during model calibration. This problem is related to the high number of parameters that need to be estimated, their correlation and the high non-linearity of the model. The automated calibration approach we used for the Taylor and Jaffé (1990a) case proved extremely useful. However, this method is time-consuming and not suitable when larger numerical domains are considered, such as for the Kildsgaard and Engesgaard (2002) case.

4. Sensitivity to initial conditions

The above model validation showed that a number of key properties of the domain play a crucial role in determining the evolution of the porosity and conductivity profile along the flow direction, and consequently in determining the bulk, effective hydraulic conductivity of the system. While some parameters can be measured or reliably estimated, others are not accessible, at least at the beginning of the experiment. A possible way to investigate the impact of unknown parameters in complex environmental models is perform a sensitivity analysis (Campolongo et al., 2007; Checchi et al., 2007; Refsgaard et al., 2007; Zoras et al., 2007, Norton 2008). In modeling bio-clogging, one difficult-to-measure property is the initial biomass distribution. In most of the experiments reported in the literature, the porous medium used is first treated to remove all the organic carbon and subsequently seeded with some selected bacterial communities. While no experimental data are available, it is reasonable to assume that the initial concentration of biomass is not homogeneous, but varies both across the longitudinal and transverse flow directions. This is evident from the experimental results of Kildsgaard and Engesgaard (2002, Figure 11). For a homogeneous initial concentration,

635 one would expect the tracer plume to be symmetric at any time, while it is not. In the simulations
636 reported above, as in the literature, we assumed a homogeneous small initial concentration of bio-
637 mass. In this section we investigate the impact of this condition on the final results, as well as the
638 additional uncertainty introduced. Also, several experiments reported a medium to large increase in
639 dispersivity together with the reduction in porosity and permeability (Taylor and Jaffé, 1990c; Bi-
640 elefeldt et al., 2002; Seifert and Engesgaard, 2007). Among the possible reasons to explain such be-
641 havior is the increased tortuosity of the flow paths as a consequence of the inhomogeneous biomass
642 growth. We will use numerical experiments to investigate the extent to which such process can con-
643 tribute to an increase of dispersivity.

644 ### *4.1 Procedure*

645 Two basic domains have been used to investigate the sensitivity of clogging development to the ini-
646 tial biomass distribution. The first setup is equivalent to that used to simulate the Taylor and Jaffé
647 (1990a) experiment in Section 3.2 above. Since it is 1D, only the inhomogeneity along the flow di-
648 rection can be studied. The underlying assumption is that concentrations are homogeneous normal
649 to flow, and remain so. The second setup consists of 2D, regular grid with cell size of 0.005 m and
650 physical dimensions of 0.05 m by 0.25 m. The same initial hydraulic properties of the 1D domain
651 were used. The flow and degradation rates were slightly decreased to allow a larger time step size to
652 be used, thus decreasing the model run-time.

653 **TABLE 4 NEAR HERE**

654 Two sets of numerical experiments were run. A summary of the main properties of the simulated
655 domains is reported in Table 4. The first group uses a 1D domain similar to that of Taylor and Jaffé
656 (1990a). The initial biomass concentration decreased with distance from the inlet. Linear, exponen-
657 tial and quadratic decreases were considered, together with a simulation were biomass was kept
658 constant. In order to be able to compare the results of the different test cases, the same immobile

biomass concentration at the inlet and outlet was used, with a different but comparable total immobile initial biomass. As an alternative, it would have been possible to use the same total biomass but different values at the inlet for each case. In our view, this would have made the comparison of the different simulations more difficult. In fact, a few numerical experiments demonstrated that the clogging rate is more sensitive to the biomass concentration near the inlet than the cumulative value. In the simulation with constant biomass instead, we selected a value so that the total biomass in the domain was comparable to the other three cases. The second group of numerical experiments made use of the 2D domain.

Different types of initial biomass distribution were tested, but in this work we report only the results obtained with two of them, since they capture the overall observed behavior. The two distributions were (i) log-uniform and (ii) log-normal. While for the log-uniform case there was no spatial correlation, i.e., the concentration of biomass in each cell did not depend on the concentration of the adjacent cells, for the log-normal distribution case spatial correlation was included. The main parameters characterizing the distributions are given in Table 5. Two examples of the initial conditions are shown in Figures 13 (log-uniform) and 15 (log-normal, correlated). For each distribution, five different realizations of the initial (immobile) biomass concentration were generated. A constant-flux boundary condition was used at the column inlet during the clogging simulation, while a fixed head boundary was set at the outlet. The bulk (effective) hydraulic conductivity was computed from the head difference between inlet and outlet at a given time step via Darcy's law. The average hydraulic head in the first strip of cells was used as the hydraulic head at the inlet. The Clement model was used to link porosity and hydraulic conductivity. Also, the sensitivity to growth rate and flow velocity was assessed, and we observed the same overall behavior regardless the values of these two parameters.

In order to study possible changes in dispersivity, for each realization at the end of the clogging simulation we simulated tracer experiments at selected time steps.

FIGURE 13 NEAR HERE

FIGURE 14 NEAR HERE

FIGURE 15 NEAR HERE

FIGURE 16 NEAR HERE

FIGURE 17 NEAR HERE

FIGURE 18 NEAR HERE

FIGURE 19 NEAR HERE

TABLE 5 NEAR HERE

4.2 Simulation results and discussion

Hydraulic concentration profiles for the 1D numerical experiments are reported in Figure 15. Linear, quadratic and exponential decreases of the biomass concentrations were considered, together with constant concentration. At the end of the simulation, the four cases exhibit a hydraulic conductivity profile with significantly different shapes, with different slopes of the clogging front. Nevertheless, in all cases the conductivity decrease near the inlet is very similar. This is not completely surprising since the growth rate of biomass and thus the clogging rate are directly dependent on concentration itself. The three cases with initial concentration decreasing towards the outlet show that both the distribution and the absolute value of biomass affect the rate and pattern of clogging development. This behavior is transient, and the differences reduce as the hydraulic conductivity decrease becomes more pronounced. This is reasonable, because biomass growth becomes progressively slower as the mobile porosity becomes the limiting factor and the detachment rate becomes larger. Due to the smaller initial biomass in the cells near the inlet, the constant concentration case underestimates the development of clogging. These observations lead to the conclusion that clog-

706 ging models are sensitive to initial conditions, at least for the cases where the immobile biomass
707 concentration is not homogeneous along the flow direction. Although there are no direct mea-
708 surements, it is reasonable to assume that this is always the case for sandy columns inoculated from
709 the inlet, as was the case for the Taylor and Jaffé (1990a) experiment. Due to filtration, most of the
710 bacterial cells remain near the inlet of the column, and only a small fraction can penetrate deeply
711 into it. Assuming a constant concentration can lead to a different pattern and rate of biomass and
712 clogging development which could, at least partially, explain some of the observed differences be-
713 tween experimental measurements and simulations.

714 The evolution with time of the hydraulic conductivity for the second group of numerical experi-
715 ments is reported in Figure 16 (log-uniform distribution) and Figure 17 (log-normal, spatially corre-
716 lated distribution). Results are reported in terms of mean value and standard deviation (vertical bar)
717 of the five realizations. While the 'mean' behavior is similar for the two distributions, the standard
718 deviation is significantly different. Simulations with log-uniform initial biomass distribution have
719 almost no variability, with the results of the five independent realizations very close to the average
720 value (Figure 16). Simulations with log-normal, spatially correlated initial biomass distributions
721 show instead a large standard deviation, i.e., the bulk conductivity of each of the five independent
722 realizations is significantly different from the mean value. Moreover, the variability is not constant.
723 It is initially small, increasing with the clogging rate (slope of hydraulic conductivity evolution with
724 time). It reaches a maximum at around 80 d, and then decreases again with a relatively small value
725 at the end of the simulation. At early times, the biomass concentration is still small, and a large
726 growth rate has a small effect only on the hydraulic conductivity and on the rate of clogging. As the
727 biomass concentration becomes larger, also the clogging rate increases and hydraulic conductivity
728 changes rapidly, thus amplifying the initial heterogeneity. After some time however, the hydraulic
729 conductivity near the inlet drops. The bulk value becomes controlled by the high resistance to flow
730 in the clogged area, and less sensitive to the hydraulic conductivity in the rest of the column. As ob-

731 served in the 1D simulations above, as the hydraulic conductivity approaches the lower limit, also
732 the clogging rate decreases, thus in turn reducing the variability. From this reasoning one can expect
733 that, as a larger part of the column becomes strongly clogged, the standard deviation reduces again
734 to a small, negligible value.

735 The large variability is clearly related to the more 'structured' pattern of initial biomass distribution,
736 when compared to the random, log-uniform case (Figure 13). The spatial correlation introduced in
737 the log-normal distribution allows the creation of preferential water flow paths. Instead, the lack of
738 structuring in the random log-uniform field results in an almost homogeneous distribution at the
739 macro-scale. A further confirmation is given by the hydraulic conductivity profile along the length
740 of the column (Figures 18 and 19). The two graphs report the average and standard deviation hy-
741 draulic conductivity along a cross-section of the column for one of the five realizations. By looking
742 at the standard deviation, it is evident that in both cases the hydraulic conductivity in the transverse
743 direction shows a variable degree of heterogeneity, which however disappears when looking at the
744 bulk behavior for the random log-uniform case.

745 These findings confirm once again the sensitivity of clogging processes to initial conditions, and to
746 immobile biomass distribution particularly. A similar behavior has often been observed in labora-
747 tory experiments, with similar setups resulting in a different value of hydraulic conductivity. On one
748 hand, our results are able to identify a source of uncertainty, thus providing new insights into the
749 clogging process. On the other hand, however, they introduce a further complexity in the model,
750 i.e., no prior assumption should be made on the biomass distribution. Instead, the initial condition
751 should be regarded as one of the model parameters, and needs to be calibrated or measured during
752 the experiment.

753 The same set of simulations was also used to investigate to what extent the increased tortuosity
754 modifies the hydrodynamic dispersivity. The breakthrough curves obtained from these simulations

overlap almost perfectly, clearly showing that the heterogeneity at this scale does not play any role in increasing the dispersivity.

5. Summary and conclusions

This work presented a new modular numerical model to simulate clogging of porous media. The work was mainly focused on bioclogging, i.e., changes of the hydraulic properties as a consequence of biomass growth and decay. Comparing numerical simulations and experimental data we found a reasonably good quantitative agreement, both under 1D and 2D water flow conditions. The numerical model can thus be used to forecast the extent of clogging in the numerous situations where this process plays an important role and cannot be neglected.

We found however a number of open issues that potentially limit the model reliability. Among the most important is the lack of robust, physically-based constitutive relationships to translate porosity changes into hydraulic conductivity modifications. Three relationships, with qualitatively different physical interpretations in how the bioclogging progresses at pore level, were unable to correctly reproduce the development of clogging during long-term experiments. Furthermore, each of the equations we used contains one or more tunable parameters with limited physical significance. Although our model validation investigation indicated that the small pores do not clog first, a lack of experimental information on the initial biomass distribution means that a definitive conclusion cannot be reached. In addition, the detailed pore scale simulations of Kapellos et al. (2007, Fig. 6) show biofilm development to be irregular, and not conforming to any simplified view of bioclogging development. Despite this, we suggest that the models used here provide a reasonable bracketing of the range of clogging possibilities, giving the possibility of providing bounds on overall behavior of porous media underling clogging.

A suite of simulations was used to investigate mesh convergence. We found that grid-independent results are extremely difficult to obtain, and even with very small grid Péclet numbers ($Pe < 1$) po-

779 rosity and hydraulic conductivity still depend on the size of the grid cells. This suggests that poten-
780 tially under some conditions mesh convergence cannot be achieved. Further research however
781 needs to be conducted to investigate this issue.

782 From a different perspective, another limitation identified by our numerical model applications is
783 the large number of parameters that need calibration. While this fact on one hand may appear as an
784 advantage, because it increases the flexibility of the model, on the other hand the non-uniqueness of
785 the inverse problem may largely reduce the effectiveness of the model as a predictive tool. This is
786 an important limitation shared with most of the process-based reactive transport models. While
787 some techniques exist to partially overcome it, in general it represents one of the major difficulties
788 in the practical use of this type of modeling approach. The code we developed was subsequently
789 applied to investigate the effect of the initial conditions on the rate and extent of hydraulic conduc-
790 tivity changes. A common assumption is that the initial concentration of biomass is homogeneous.
791 This is certainly a simplification, because it is likely that even under well-controlled laboratory
792 conditions the distribution of biomass shows some degree of heterogeneity. We tested the effect of
793 this assumption by comparing the evolution of the hydraulic conductivity with time starting from
794 different initial conditions, and found that the results are sensitive to this factor. In particular, we
795 observed the largest degree of variability in the simulations where the initial biomass concentration
796 was a log-normal spatially correlated random distribution. This finding has important consequences
797 for modeling because it shows that quantitative prediction of the extent and rate of bioclogging is
798 possible only when the initial conditions are well characterized.

799 Acknowledgements

800 We gratefully acknowledge P. Engesgaard for providing us with the experimental data of Kildsgaard
801 and Engesgaard (2002).

Bibliography

Amos, R., Mayer, K., 2006. Investigating the role of gas bubble formation and entrapment in contaminated aquifers: Reactive transport modelling. J. Contam. Hydrol., 87, 123-154.

Arnon, S., Adar, E., Ronen, Z., Yakirevich, A., Nativ, R., 2005. Impact of microbial activity on the hydraulic properties of fractured chalk. J. Contam. Hydrol., 76, 315-336.

Barry, D.A., Miller, C., Culligan, P., Bajracharya, K., 1997. Analysis of split operator methods for nonlinear and multispecies groundwater chemical transport models. Math. Comp. Simul., 43, 331-341.

Barry, D.A., Prommer, H., Miller, C., Engesgaard, P., Brun, A., Zheng, C., 2002. Modelling the fate of oxidisable organic contaminants in groundwater. Adv. Water Res., 25, 945-983.

Bajracharya, K., Barry, D. A., 1995. MCMFIT: Efficient optimal fitting of a generalised nonlinear advection-dispersion model to experimental data. Comput. Geosci. 21, 61-76.

Baveye, P., Valocchi, A., 1989. An evaluation of mathematical models of the transport of biologically reacting solutes in saturated soils and aquifers. Water Resour. Res., 25, 1413-1421.

Baveye, P., Vandevivere, P., Hoyle, B., DeLeo, P., Lozada, D.S., 1998. Environmental impact and mechanisms of the biological clogging of saturated soils and aquifer materials. Crit. Rev. Env. Sci. Tech. 28, 123-191.

Bielefeldt, A., Illangasekare, T., Uttecht, M., LaPlante, R., 2002. Biodegradation of propylene glycol and associated hydrodynamic effects in sand. Water Res., 36, 1707-1714.

Breadford, S.A., Simunek, J., Bettahar, M., Genuchten, M.T.V., Yates, S.R., 2003. Modeling colloid attachment, straining, and exclusion in saturated porous media. Environ. Sci. Tech.., 37, 2242-

823 2250.

824 Brovelli, A., Mao, X., Barry, D.A., 2007. Numerical modeling of tidal influence on density-depen-
825 dent contaminant transport, Water Resour. Res., 43, W10426, doi:10.1029/2006WR005173.

826 Campolongo, F., Cariboni, J. and Saltelli A. 2007. An effective screening design for sensitivity
827 analysis in large models. Environ. Model. Soft. 22, 1509-1518.

828 Checchi, N., Giusti, E., Marsili-Libelli S. 2007. PEAS: A toolbox to assess the accuracy of esti-
829 mated parameters in environmental models. Environ. Model. Soft. 22, 899-913.

830 Clement, T.P., Hooker, B.S., Skeen, R.S., 1996. Macroscopic models for predicting changes in satu-
831 rated porous media properties caused by microbial growth. Ground Water, 34, 934-942.

832 Clement, T.P., Peyton, B., Skeen, R.S., Jennings, D., Petersen, J., 1997. Microbial growth and trans-
833 port in porous media under denitrification conditions: Experiments and simulations. J. Contam.
834 Hydrol., 24, 269-285.

835 Dai, Z., Samper, J., 2004. Inverse problem of multicomponent reactive chemical transport in porous
836 media: formulation and applications. Water Resour. Res, 40, W07407.

837 Doherty, J., 2004. PEST. Model-Independent Parameter Estimation. User Manual: 5th edition. Wa-
838 termark Numerical Computing, Australia. .http://www.sspa.com/pest (Accessed DATE).

839 Dupin, H., Kitanidis, P., McCarty, P., 2001. Pore-scale modeling of biological clogging due to ag-
840 gregate expansion: A material mechanics approach. Water Resour. Res., 37, 2965-2979.

841 Ford, R., Harvey, R., 2007. Role of chemotaxis in the transport of bacteria through saturated porous
842 media. Adv. Water Resour, 30, 1608-1617.

843 Gargiulo, G., Bradford, S., Simunek, J., Ustohal, P., Vereecken, H., Klupp, E., 2007. Bacteria trans-

844 port and deposition under unsaturated conditions: The role of the matrix grain size and the bac-
845 teria surface protein. J. Contam. Hydrol., 92, 255-273.

846 Guo, W., Langevin, C., 2002. User's guide to SEAWAT: a computer program for simulation of
847 three-dimensional variable-density ground-water flow. U.S Geological Survey Techniques of
848 Water resources Investigations Book 6, USA.

849 Ham, Y., Kim, S., Park, S., 2007. Numerical experiments for bioclogging in porous media. Environ.
850 Technol., 28, 1079-1089.

851 Harvey, R., Garabedian, S., 1991. Use of colloid filtration theory in modeling movement of bacteria
852 through a contaminated sandy aquifer. Environ. Sci. Technol., 25, 178-185.

853 Hornberger, G., Mills, A., Herman, J., 1992. Bacterial transport in porous media: evaluation of a
854 model using laboratory observations. Water Resour. Res., 28, 915-938.

855 Islam, J., Singal, N., O'Sullivan, M., 2001. Modeling biogeochemical processes in leachate-
856 contaminated soils: a review. Transp. Porous Media, 43, 407-440.

857 Ives, K., Pienvichitr, V., 1965. Kinetics of the filtration of dilute suspensions. Chem. Eng. Sci., 20,
858 965-973.

859 Jiang, G., Noonan, M., Buchan, G., Smith, N., 2007. Transport of Escherichia coli through variably
860 saturated sand columns and modeling approaches. J. Contam. Hydrol., 93, 2-20.

861 Kapellos, G., Alexiou, T. and Payatakes, A., 2007. Hierarchical simulator of biofilm growth and dy-
862 namics in granular porous materials. Adv. Water Res., 30, 1648-1667.

863 Kildsgaard, J., Engesgaard, P., 2001. Numerical analysis of biological clogging in two-dimensional
864 sand box experiments. J. Contam. Hydrol., 50, 261-285.

865 Kildsgaard, J., Engesgaard, P., 2002. Tracer tests and image analysis of biological clogging in a
866 two-dimensional sandbox experiment. Ground Water Monit. Remed., 60, 60-67.

867 Kim, Y.S., Whittle, A.J., 2006. Filtration in a porous granular medium: 1. Simulation of pore-scale
868 particle deposition and clogging. Transp. Porous Media, 65, 53-87.

869 Kindred, J., Celia, M., 1989. Contaminant transport and biodegradation. 2. Conceptual model and
870 test simulation. Water Resour. Res., 25, 1149–1160.

871 Knapp, R., Civan, F., McInerney, M., 1988. Modeling growth and transport of microorganisms in
872 porous formations. In Vichnevetsky, R., Borne, P., Vignes, J. (Eds), 12th IMACS World Con-
873 gress on Scientific Computation, IMACS 1988. Vol. 3, 676-679

874 Magid, J., De Neergaard, A., Brandt, M., 2006. Heterogeneous distribution may substantially de-
875 crease initial decomposition, long-term microbial growth and N-immobilization from high C-
876 to-N ratio resources. Eur. J. Soil Sci., 57, 517-529.

877 Mao, X., Prommer, H., Barry, D.A., Langevin, C., Panteleit, B., 2006. Three-dimensional model for
878 multi-component reactive transport with variable density groundwater flow. Environ. Model.
879 Soft., 21, 615-628.

880 McDonald, M., Harbaugh, A., 1988. A Modular three-dimensional finite-difference ground-water
881 flow model. U.S Geological Survey, USA.

882 Miralles-Wilhelm, F., Gelhar, L.W., Kapoor, V., 1997. Stochastic analysis of oxygen-limited biode-
883 gradation in three-dimensional heterogeneous aquifers. Water Resour. Res. 33, 1251-1263.

884 Mohamed, M.A.M., Hatfield, K., Hassan, A.E., 2006. Monte Carlo evaluation of microbial-me-
885 diated contaminant reactions in heterogeneous aquifers. Adv. Water Resour., 29, 1123-1139.

886 Molz, F., Widdowson, M., Benefield, L., 1986. Simulation of microbial growth dynamics coupled

887 to nutrient and oxygen transport in porous media. Water Resour. Res., 22, 1207-1216.

888 Norton, J.P., 2008. Algebraic sensitivity analysis of environmental models. Environ. Model. Soft.
889 23, 963-972.

890 O'Melia, C.R., Ali, W., 1978. The role of retained particles in deep bed filtration. Prog. Water Tech.,
891 10, 167-182.

892 Okubo, T., Matsumoto, J., 1979. Effect of infiltration rate in biological clogging and water quality
893 changes during artificial recharge. Water Resour. Res., 15, 1536-1542.

894 Parkhurst, D., Appelo, C., 1999. User's guide to PHREEQC - A computer program for speciation,
895 reaction-path, 1D transport and inverse geochemical calculations. U.S Geological Survey,
896 USA.

897 Pavelic, P., Dillon, P.J., Barry, K.E., Vanderzalm, J.L., Correll, R.L., Rinck-Pfeiffer, S.M. 2007. Wa-
898 ter quality effects on clogging rates during reclaimed water ASR in a carbonate aquifer. J. Hy-
899 drol., 334, 1-16.

900 Prommer, H., Barry, D.A., 2005. Modeling bioremediation of contaminated groundwater. In Atlas
901 R. and Philp J.C. (Eds.), Bioremediation: Applied microbial solutions for real-world environ-
902 mental clean-up., pp. 108-138.

903 Prommer, H., Barry, D.A., Davis, G., 1999a. A one-dimensional reactive multi-component transport
904 model for biodegradation of petroleum hydrocarbons in groundwater. Environ. Model. Soft-
905 ware, 14, 213-223.

906 Prommer, H., Barry, D.A., Zheng, C., 2003. MODFLOW/MT3DMS-based reactive multi-compo-
907 nent transport modeling. Ground Water, 41, 247-257.

908 Prommer, H., Davis, G., Barry, D.A. 1999b. PHT3D — A three-dimensional biogeochemical trans-

port model for modelling natural and enhanced remediation. In Johnston C.D. (Ed.), Proc. Contaminated site remediation: Challenges posed by urban and industrial contaminants, Fremantle, WA, Australia, 21–25 March, 1999. pp. 351–358.

Prommer, H., Davis, G., Barry, D.A., 2000. Biogeochemical transport modelling of natural and enhanced remediation processes in aquifers. Land Contam. Reclam., 8, 217-223.

Reddi, L., Ming, X., Hajra, M., Lee, I., 2000. Permeability reduction of soil filters due to physical clogging. J. Geotech. Geoenviron. Eng., 126, 236-246.

Refsgaard, J.C., van der Sluijs, J.P., Hoiberg A.L., Vanrolleghem P.A. 2007. Uncertainty in the environmental modelling process. A framework and guidance. Environ. Model. Soft. 22, 1543-1556.

Rittmann, B., 1982. The effect of shear stress on biofilm loss rate. Biotech. and Bioeng., 24, 501-506.

Sahimi, M., 1995. Flow and Transport in Porous Media and Fractured Rock. VCH Verlagsgesellschaft, Weinheim, Germany.

Scheibe, T., Dong, H., Xie, Y., 2007. Correlation between bacterial attachment rate coefficients and hydraulic conductivity and its effect on field-scale bacterial transport. Adv. Water Res., 30, 1571-1582.

Scholl, M.A., 2000. Effects of heterogeneity in aquifer permeability and biomass on biodegradation rate calculations. Results from numerical simulations. Ground Water, 38, 702-712.

Seifert, D., 2005. Experimental and numerical investigations of changes in flow and solute transport processes in porous media affected by bioclogging, PhD Thesis, Danish Technical University, Copenhagen.

931 Seifert, D., Engesgaard, P., 2007. Use of tracer tests to investigate changes in flow and transport
932 properties due to bioclogging of porous media. J. Contam. Hydrol., 93, 58-71.

933 Seki, K., Miyazaki, T., Nakano, M., 1998. Effects of microorganisms on hydraulic conductivity de-
934 crease in infiltration. Eur. J. Soil Sci., 49, 231-236.

935 Seki, K., Thullner, M., Miyazaki, T., 2006. Moderate bioclogging leading to preferential flow paths
936 in biobarriers. Ground Water Monitor. Remed., 26, 68-76.

937 Shawn Matott, L., Rabideau, A.J., 2008. Calibration of subsurface batch and reactive-transport
938 models involving complex biogeochemical processes. Adv. Water Res., 31, 269-286.

939 Sleep, B., Seepersad, D., Mo, K., Heidorn, C., Hrapovic, L., Morrill, P., McMaster, M., Hood, E.,
940 Lebron, C., Lollar, B., Major, D., Edwards, E., 2006. Biological enhancement of tetrachloroe-
941 thene dissolution and associated microbial community changes. Environ. Sci. Technol., 40,
942 3623-3633.

943 Tan, Y., Gannon, J., Baveye, P., Alexander, M., 1994. Transport of bacteria in an aquifer sand: Expe-
944 riments and model simulations. Water Resour. Res., 30, 3243-3252.

945 Taylor, S.W., Jaffé, P.R., 1990a. Biofilm growth and the related changes in the physical properties
946 of a porous medium. 1. Experimental investigation. Water Resour. Res., 26, 2153-2159.

947 Taylor, S.W., Milly, P., Jaffé, P.R., 1990b. Biofilm growth and the related changes in the physical
948 properties of a porous medium. 2. Permeability. Water Resour. Res., 26, 2161-2169.

949 Taylor, S.W., Jaffé, P.R., 1990c. Biofilm growth and the related changes in the physical properties
950 of a porous medium. 3. Dispersivity and model verification. Water Resour. Res., 26, 2171-
951 2180.

952 Taylor, S.W., Jaffé, P.R., 1990d. Substrate and biomass transport in a porous medium. Water Resour.

953 Res., 26, 2181-2194.

954 Thullner, M., Mauclaire, L., Schroth, M.H., Kinzelbach, W., Zeyer, J., 2002a. Interaction between
955 water flow and spatial distribution of microbial growth in a two-dimensional flow field in satu-
956 rated porous media. J. Contam. Hydrol., 58, 169-189.

957 Thullner, M., Schroth, M.H., Zeyer, J. Kinzelbach, W., 2004. Modeling of a microbial growth expe-
958 riment with bioclogging in a two-dimensional saturated porous media flow field. J. Contam.
959 Hydrol., 70, 37-62.

960 Thullner, M., Zeyer, J., Kinzelbach, W. 2002b. Influence of microbial growth on hydraulic proper-
961 ties of pore networks. Transp. Porous Media, 49, 99-122.

962 Tien, C., Turian, R., Pandse, H., 1979. Simulation of the dynamics of deep-bed filters. AIChEJ, 25,
963 385-395.

964 Tufenkji, N., 2007. Modeling microbial transport in porous media: Traditional approaches and re-
965 cent developments. Adv. Water Resour., 30, 1455-1469.

966 Vandevivere, P., Baveye, P., 1992. Effect of bacterial extracellular polymers on the saturated hy-
967 draulic conductivity of sand columns. App. Env. Microbiol., 58, 1690-1698.

968 Vandevivere, P., Baveye, P., Lozada, D., DeLeo, P., 1995. Microbial clogging of saturated soils and
969 aquifer materials: Evaluation of mathematical models. Water Resour. Res., 31, 2173-2180.

970 VanGulck, J.F., Rowe, R., 2004. Evolution of clog formation with time in columns permeated with
971 synthetic landfill leachate. J. Contam. Hydrol., 75, 115-139.

972 Wantanaphong, J., Mooney, S., Bailey, E., 2006. Quantification of pore clogging characteristics in
973 potential permeable reactive barrier (PRB) substrates using image analysis. J. Contam. Hydrol.,
974 86, 299-320.

975 Zheng, C., Bennett, G., 2002. Applied Contaminant Transport Modelling, Second edition. Wiley-In-
976 terscience, New York, USA.

977 Zheng, C., Wang, P., 1999. MT3DMS, a modular three-dimensional multi-species transport model
978 for simulation of advection, dispersion and chemical reactions of contaminants in ground-water
979 systems; Documentation and user's guide. U.S. Army Engineer Research and Development
980 Center, USA.

981 Zoras S., Triantafyllou, A.G., Hurley P.J. 2007. Grid sensitivity analysis for the calibration of a
982 prognostic meteorological model in complex terrain by a screening experiment. Environ. Mod-
983 el. Soft. 22, 33-39.

984 Zysset, A., Stauffer, F., Dracos, T., 1994. Modeling of reactive groundwater transport governed by
985 biodegradation. Water Resour. Res., 30, 2423-2434.

Tables

Table 1. Summary of the properties of the column experiment by Taylor and Jaffé (1990a).

Parameter	Value
Column length	0.52 m
Column diameter	0.0508 m
Mean grain diameter	7×10^{-4} m
Grain diameter range	5.9×10^{-4} - 8.4×10^{-4} m
Porosity	0.347
Specific surface	485 m^{-1}
Initial hydraulic conductivity	217 m d^{-1}
Influent substrate concentration	7.2 mg l^{-1}
Flow rate	1.915 m^3 d^{-1}

Table 2. Summary of the numerical experiments conducted to investigate the effects of resolution and dispersivity on the accuracy.

Case	ΔL [m]	α_L [m]	*Pe*	Relative error, porosity	Relative error, conductivity
A	10^{-2}	5×10^{-3}	2		
				13%	45%
B	5×10^{-3}	5×10^{-3}	1		
C	10^{-2}	5×10^{-2}	0.5		
				3%	8%
D	5×10^{-3}	5×10^{-2}	0.1		

8 Table 3. Summary of the properties of the sandbox experiment (Kildsgaard and Engesgaard, 2002).

Parameter	Value
Box length	0.44 m
Box width	0.3 m
Box thickness	0.01 m
Porosity	0.39
Grain size (d_{10})	3.2×10^{-4} m
Initial hydraulic conductivity	84.7 m d^{-1}
Longitudinal dispersivity (α_L)	7.7×10^{-4} m
Transversal dispersivity (α_T)	6×10^{-5} m
Concentration, $CH_3COONa \cdot 3H_20$	90 mg l^{-1}
Concentration, KNO_3	90 mg l^{-1}
Background flow rate	9.6 l d^{-1}
Solution flow rate	0.72 l d^{-1}

9

10 Table 4. Main properties of the simulated domains in the experiments conducted to investigate the sen-
11 sitivity of clogging to initial conditions.

Properties	1D simulations	2D simulations
Domain length	2.5×10^{-1} m	2.5×10^{-1} m
Domain width	5×10^{-3} m	5×10^{-2} m
Domain thickness	5×10^{-3} m	5×10^{-3} m
Grid resolution	5×10^{-3} m	5×10^{-3} m
Starting porosity	0.35	0.35
Starting hydraulic conductivity	215 m d^{-1}	215 m d^{-1}
Maximum growth rate	9×10^{-7} d^{-1}	9×10^{-7} d^{-1}
Half-saturation constant	8×10^{-4} mol l^{-1}	8×10^{-4} mol l^{-1}
Yield factor	0.2	0.2

12

13 Table 5. Properties of the log-normal random distribution of biomass. The correlation lengths are rela-
14 tive to the total size of the domain.

Property	Log-normal distribution	Log-uniform distribution
Biomass concentration, mean value (logarithm base 10)	-2.8	
Biomass concentration, standard deviation (logarithm base 10)	-0.6	
Biomass concentration, range		10^{-5} – 10^{-1} mg l^{-1}
Correlation length, longitudinal	0.4	
Correlation length, transversal	0.4	

15

Figures

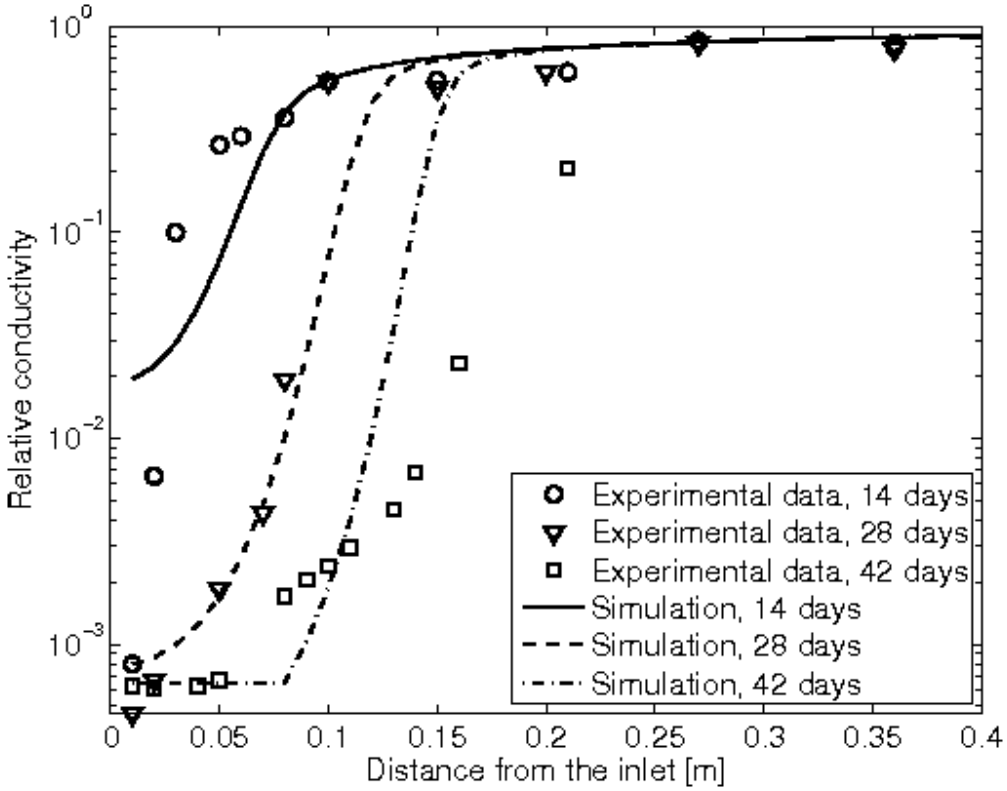

Figure 1. Comparison of the 1-D simulations with the experimental data from Taylor and Jaffé (1990a). The experimental data at time 14 and 28 d were used for calibration, while the results at 42 d are used for model validation.

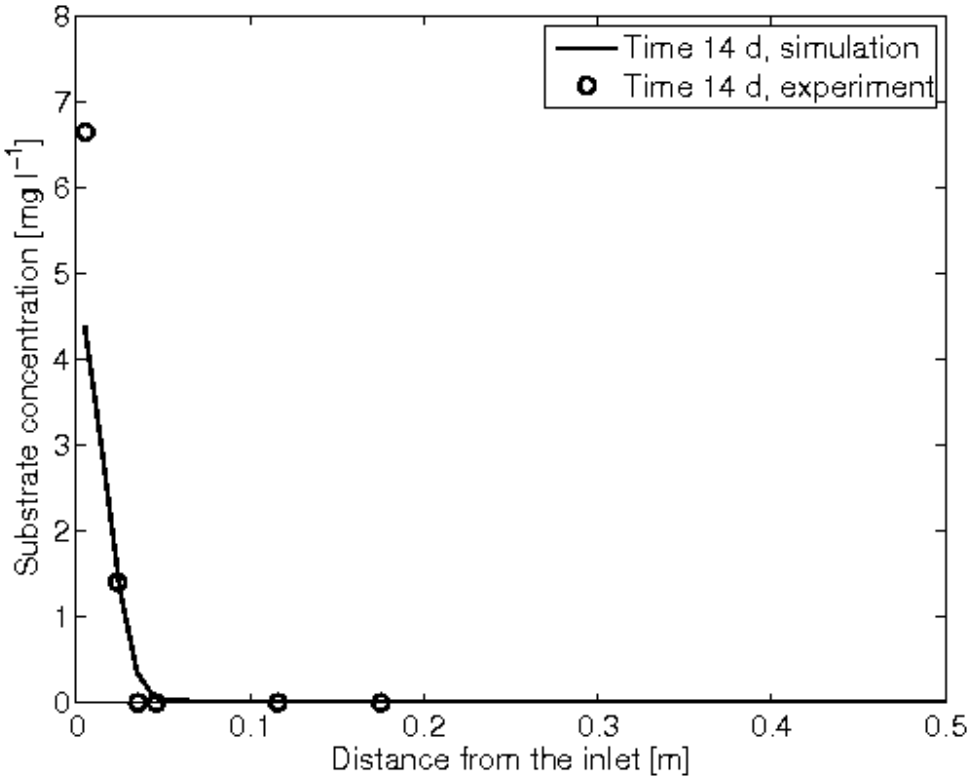

Figure 2. Measured and simulated substrate concentrations at 14 d. The substrate data were not used during calibration. The good agreement indicates successful calibration of the model.

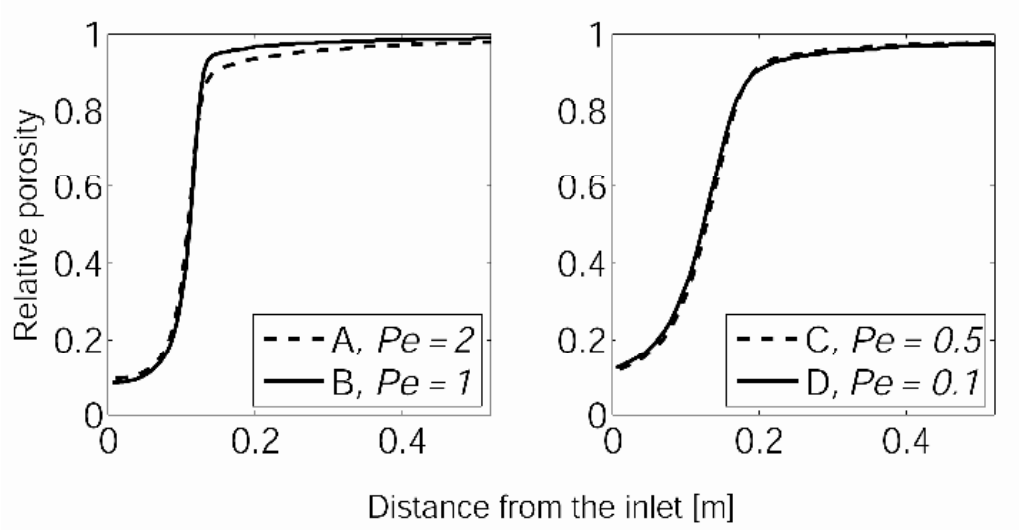

24

25 Figure 3. Effect of the *Pe* on the simulated porosity. Time is 28 d. The capital letters A, B, C, D refer to

26 the cases described in Table 2. Even for very small *Pe* values some small discrepancies are observed.

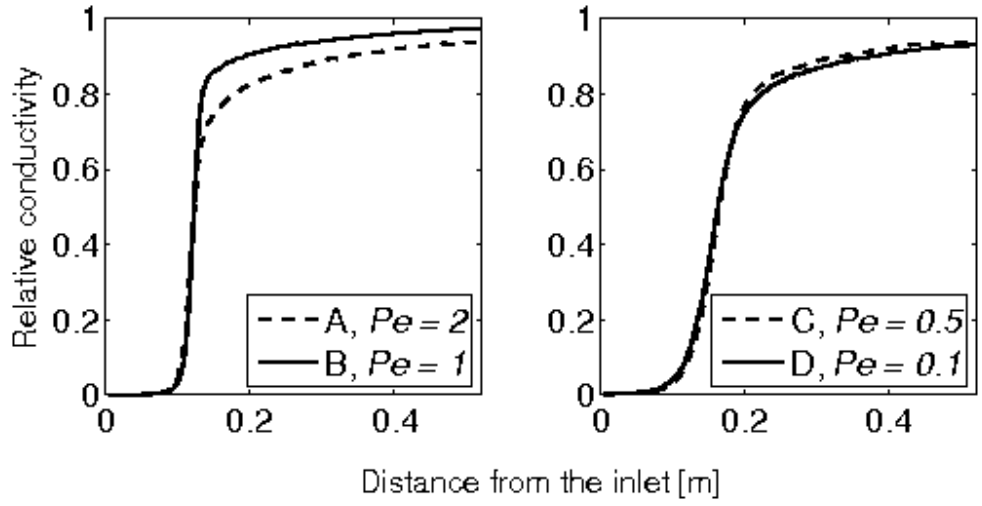

Figure 4. Effect of *Pe* on the simulated hydraulic conductivity. Time is 28 d. The capital letters A, B, C, D refer to the cases described in Table 2. Due to the exponential relationship between porosity and hydraulic conductivity, the errors are larger than in Figure 4. This indicates that a small *Pe* value is necessary to capture correctly the evolution of the clogging process.

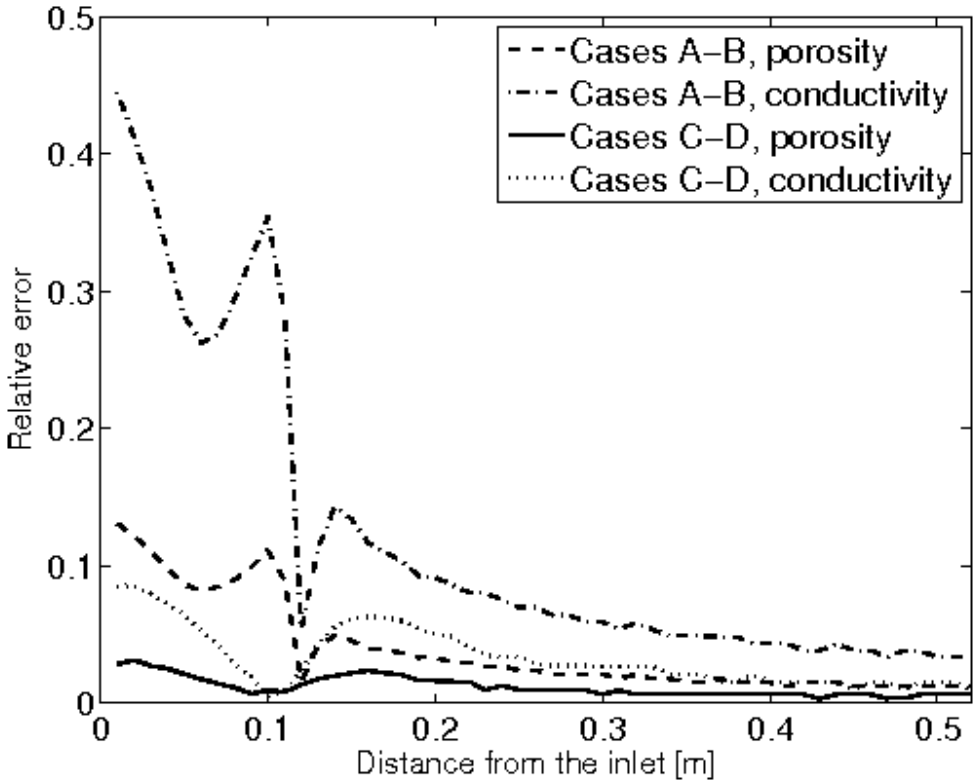

32 Figure 5. Relative error between the simulations with different *Pe* values.

33

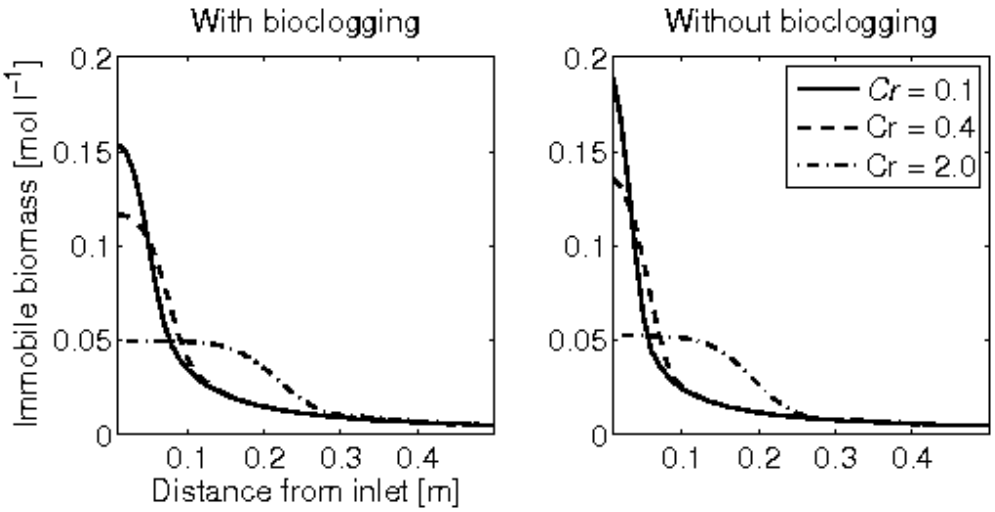

34 Figure 6. Immobile biomass distribution inside the column for the 1D simulation. Results of the simu-

35 lations with and without clogging are reported using different time steps. Due to the increase in flow
36 velocity as a consequence of clogging, the biomass concentration near the inlet is lower when clogging
37 is activated.
38

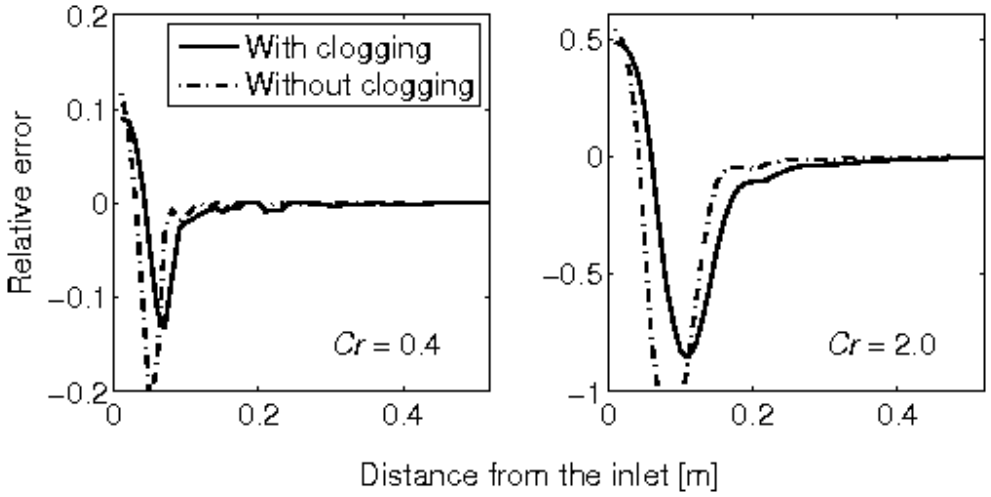

Figure 7. OSE for different Courant numbers. The biomass concentration is compared to the values obtained with $Cr = 0.1$. The error is less pronounced when the simulation includes clogging.

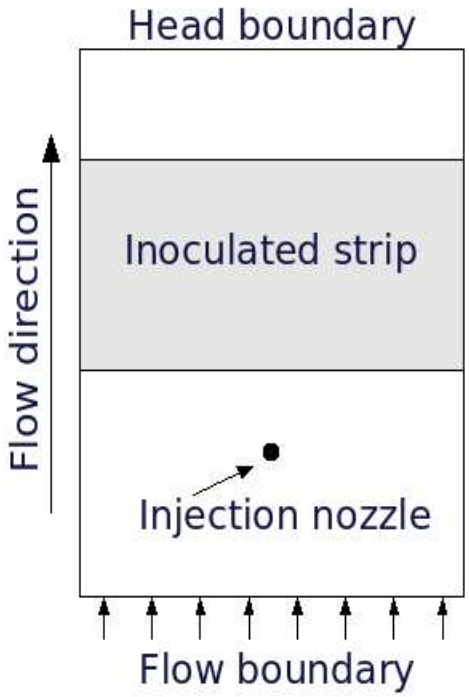

Figure 8. Schematic representation of the experimental set-up of Kildsgaard and Engesgaard (2001).

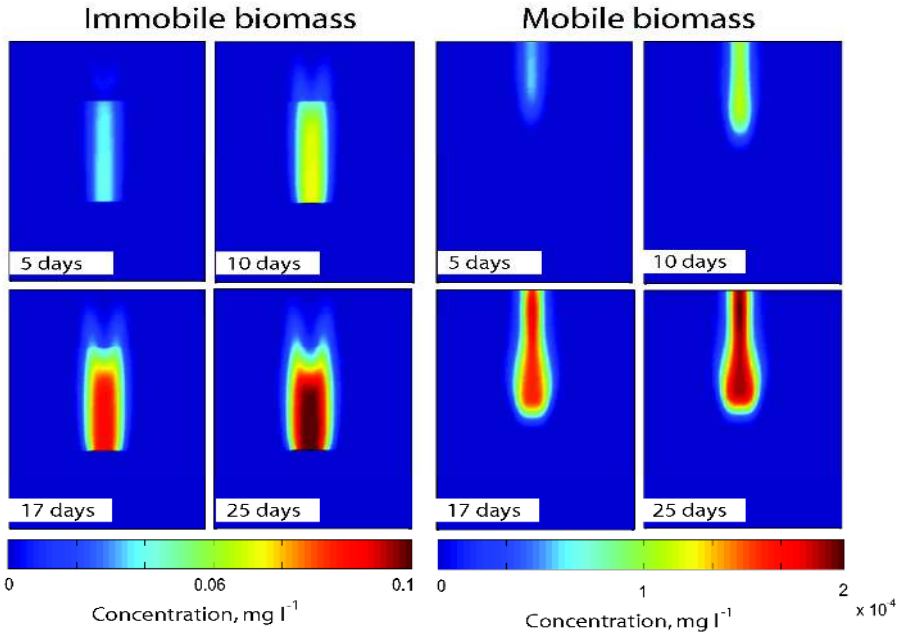

43

44 Figure 9. Mobile (left panel) and immobile (right panel) biomass concentrations using the constitutive

45 relationship of Clement et al. (1996). The flow direction is top to bottom.

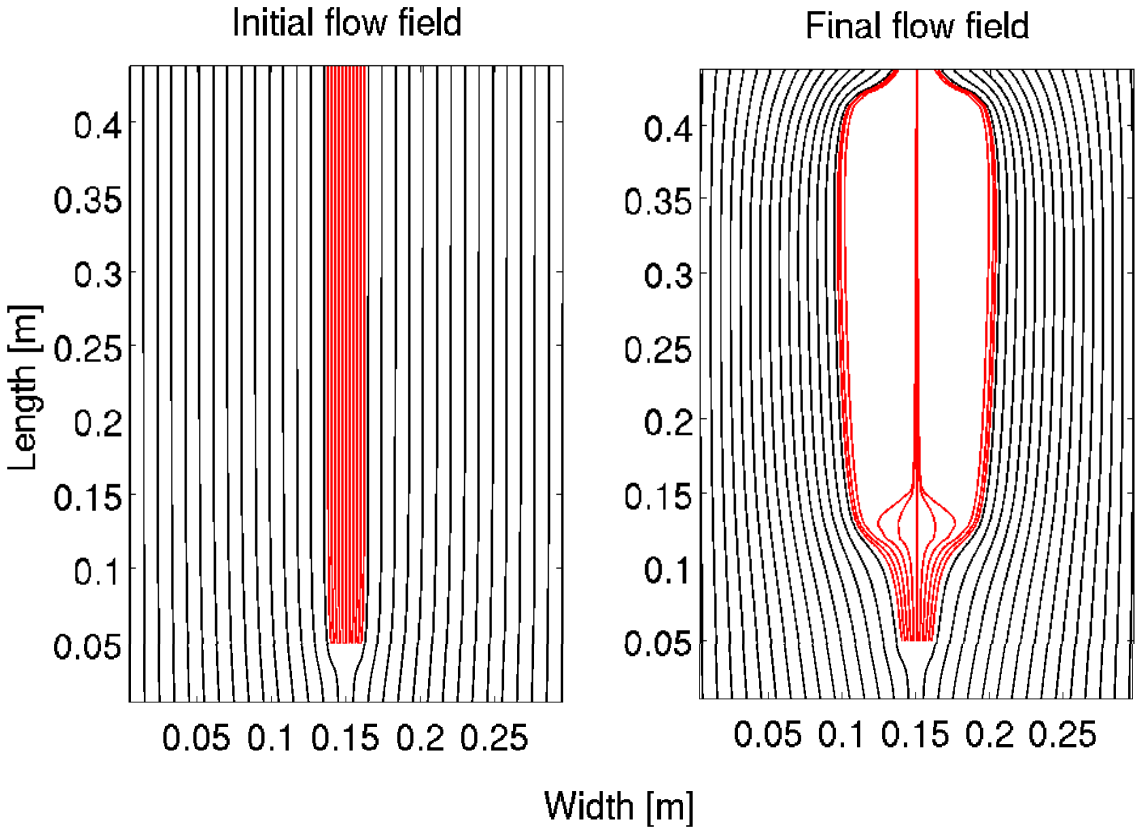

Figure 10. Initial and final simulated flow field for the Kildsgaard and Engesgaard (2002) case. The flow lines in black show the trajectory of the background water, while the lines drawn in red are relevant to the water injected from the nozzle. The disturbance to flow induced by clogging is clear, with little or no water flowing through the zone with higher biomass concentration.

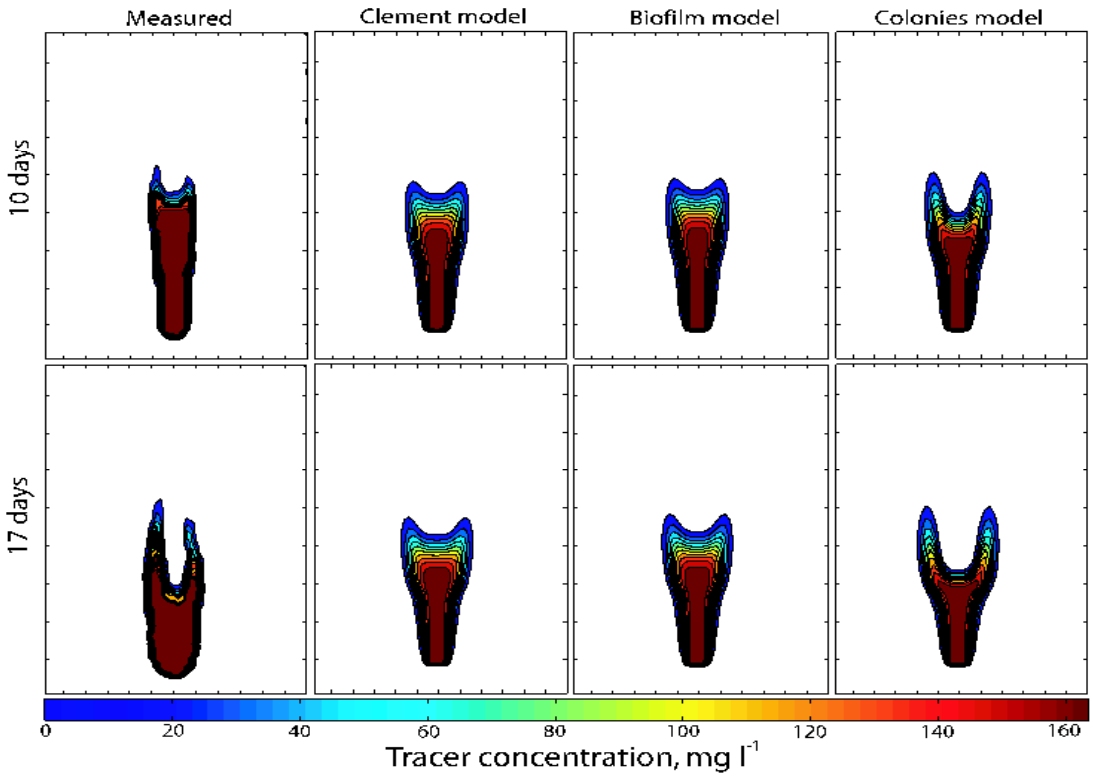

Figure 11. Simulation results for the Kildsgaard and Engesgaard (2002) case. The first column shows the experimental result, while the other three columns are relevant to different constitutive equations for the porosity-hydraulic conductivity relationship. The Clement and biofilm models show better agreement at early times (up to about 10 d), while the colonies model better reproduces the experimental data when clogging is more pronounced.

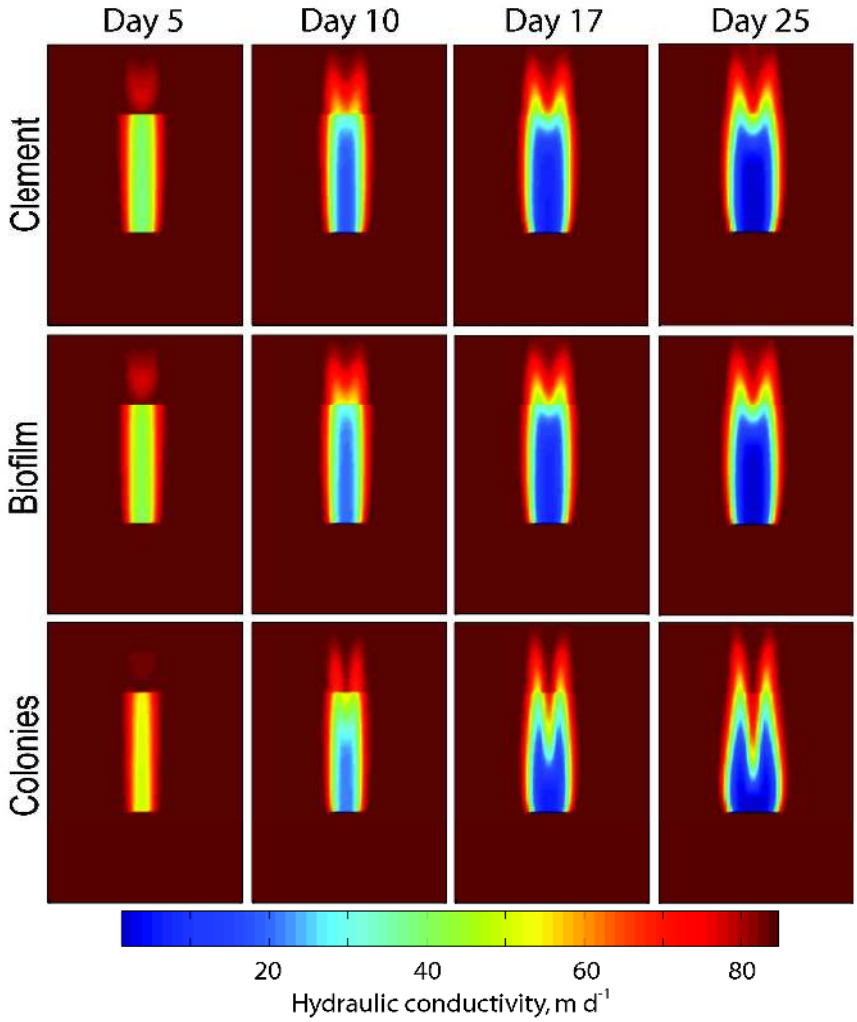

Figure 12. Evolution of the hydraulic conductivity with time (5, 10, 17 and 25 d) for the three constitutive relationships used in this work. The shape of the clogged zone for the biofilm and Clement relationship is similar, while it significantly differs for the colonies model.

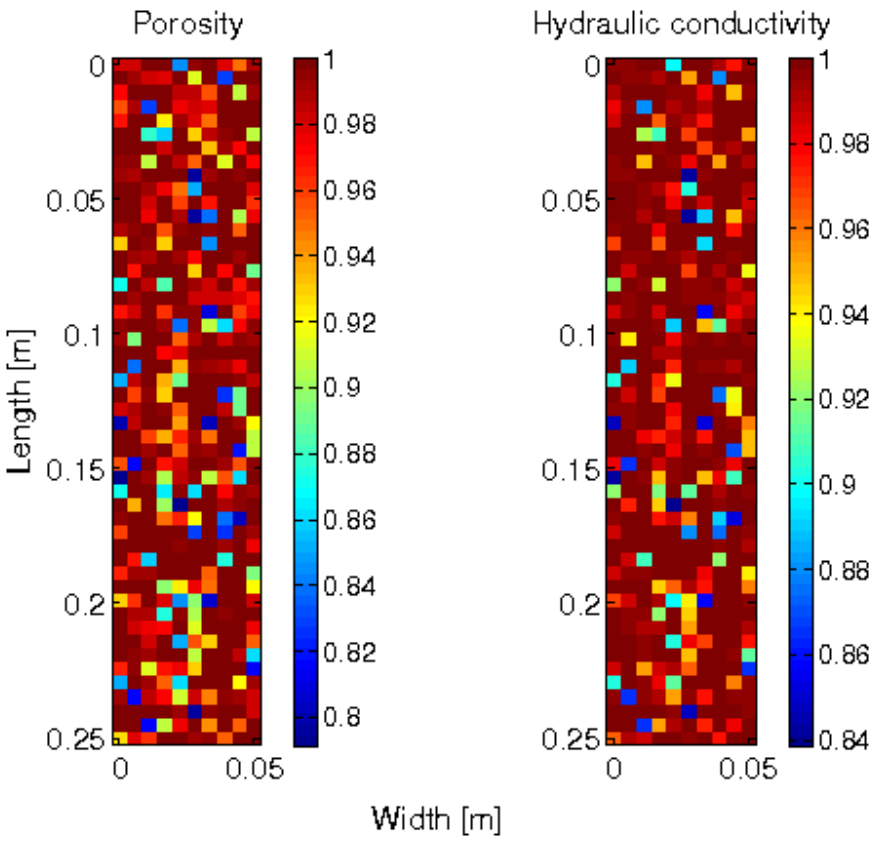

Figure 13. Example of the initial porosity and hydraulic conductivity using a log-uniform, uncorrelated distribution of biomass. Porosity and hydraulic conductivity values are normalized with respect to the original (i.e., clean sand) values.

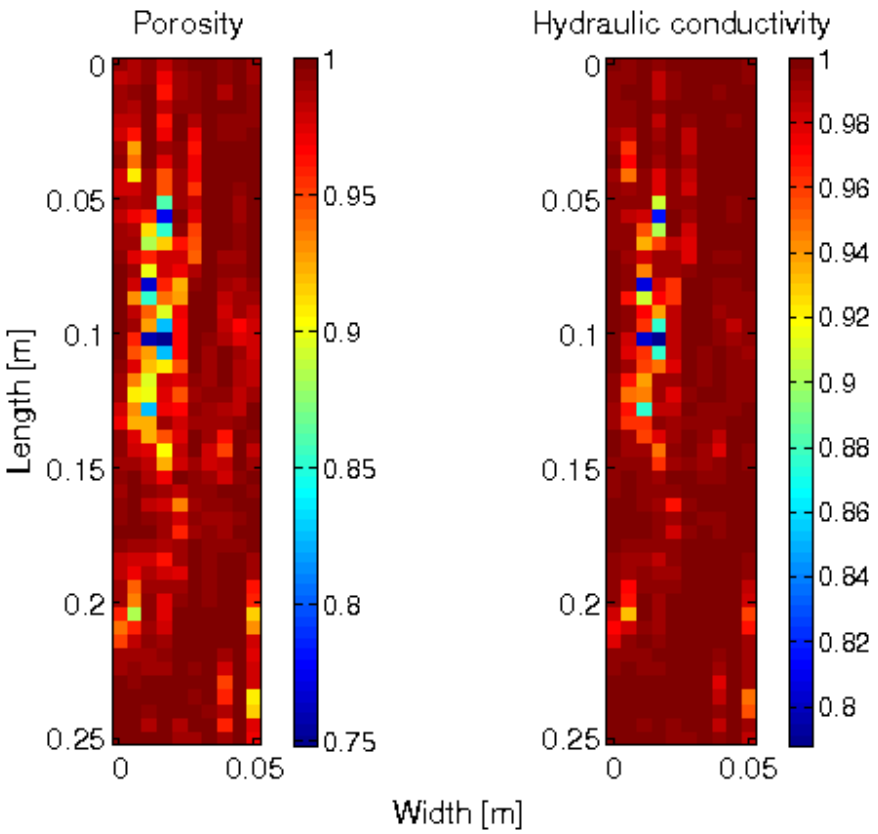

Figure 14. Example of the initial porosity and hydraulic conductivity using a log-normal, spatially correlated distribution of biomass. Porosity and hydraulic conductivity values are normalized with respect to the original (i.e., clean sand) values.

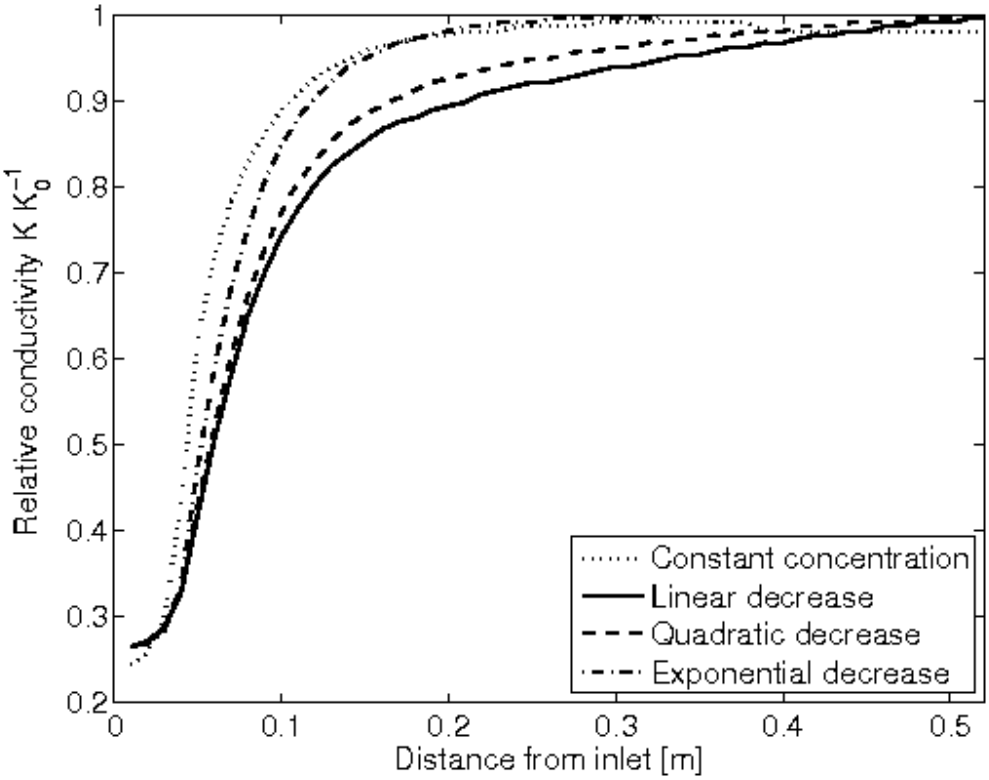

Figure 15. Hydraulic conductivity variations along the length of the column (after 28 d). Three initial biomass distributions are used. The initial concentration of biomass is homogeneous across the transverse direction, and decreases from the inlet to the outlet of the column. Different initial conditions result in a different hydraulic conductivity profile and thus in a different bulk value.

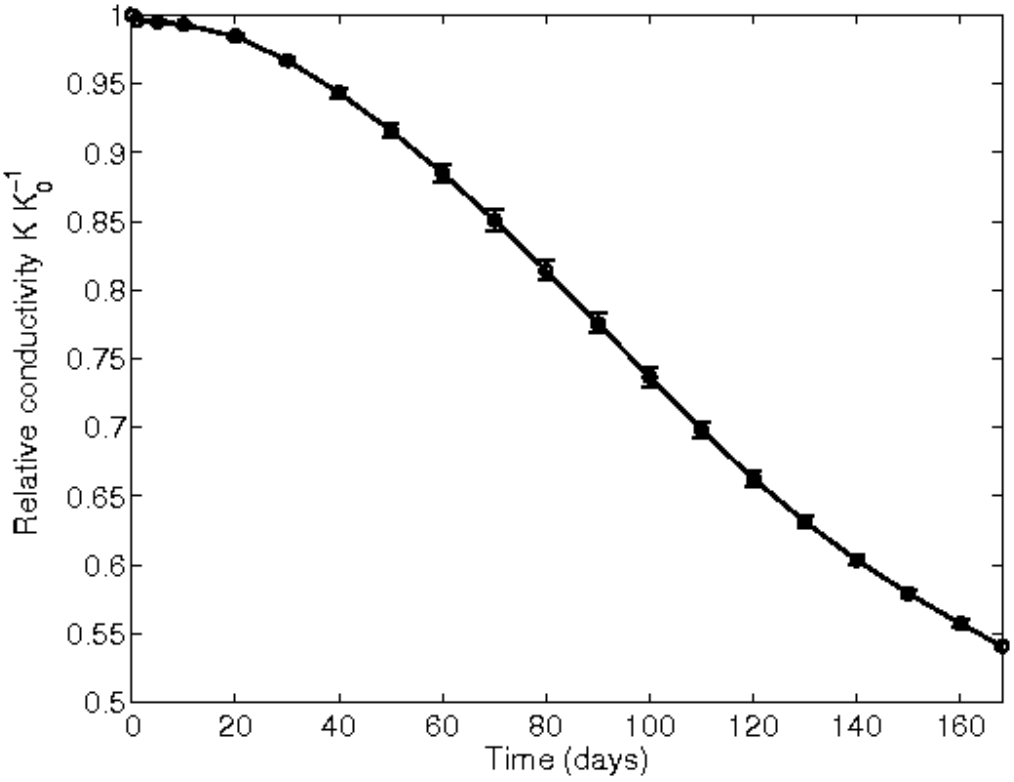

Figure 16. Evolution of the hydraulic conductivity with time using a random, uncorrelated initial distribution of biomass. Porosity and hydraulic conductivity values are normalized with respect to the original (i.e., clean sand) values. Mean value and standard deviation of five realizations are shown.

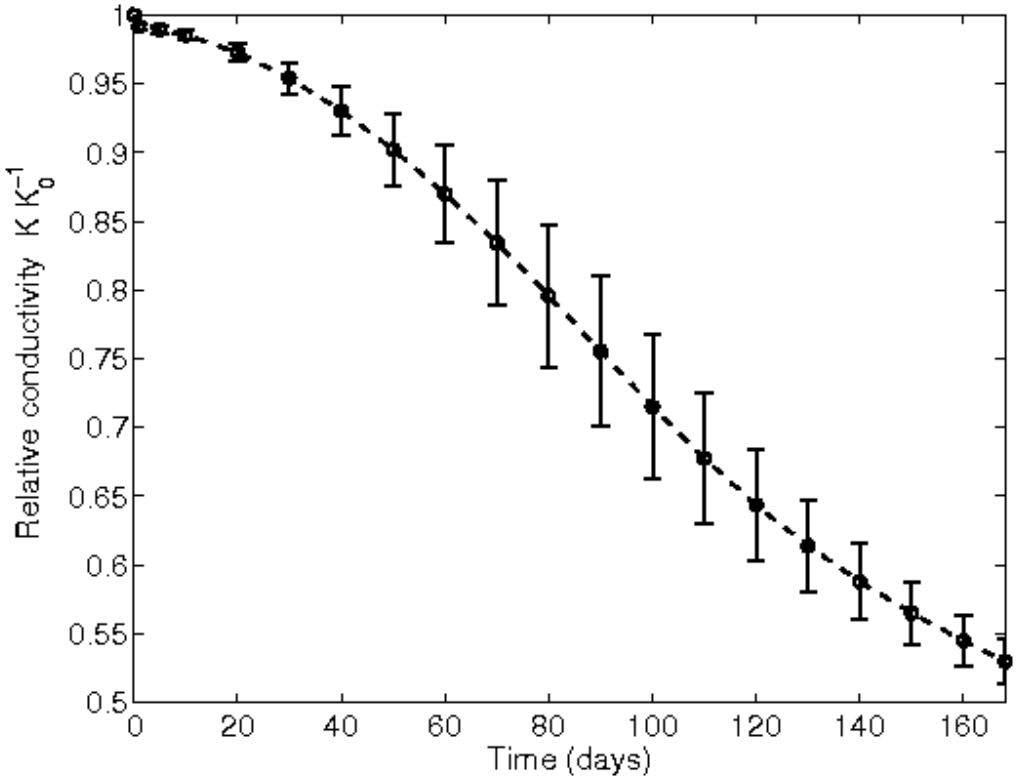

77 Figure 17. Evolution of the hydraulic conductivity with time using a log-normal, spatially correlated
78 distribution of biomass. Porosity and hydraulic conductivity values are normalized with respect to the
79 original (i.e., clean sand) values. Mean value and standard deviation of five realizations are shown.
80

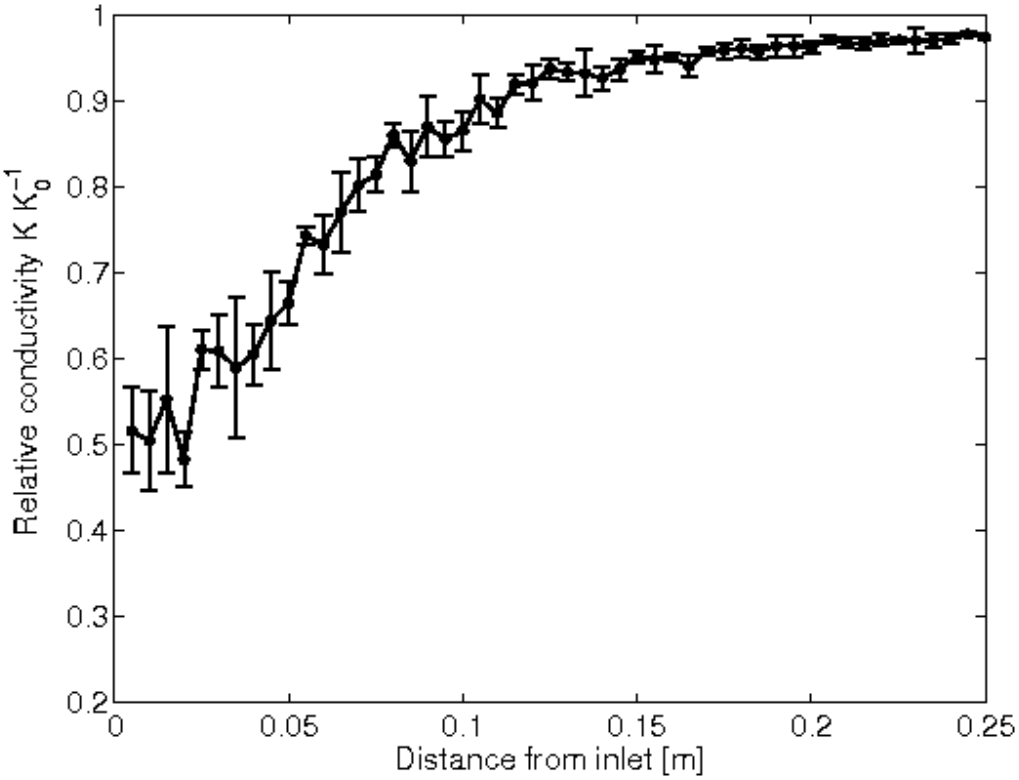

81 Figure 18. Spatial profile of the hydraulic conductivity along the length of the column. For each cross-
82 section, the mean value and the standard deviation are reported. Initial biomass distribution is log-uni-
83 form, uncorrelated.

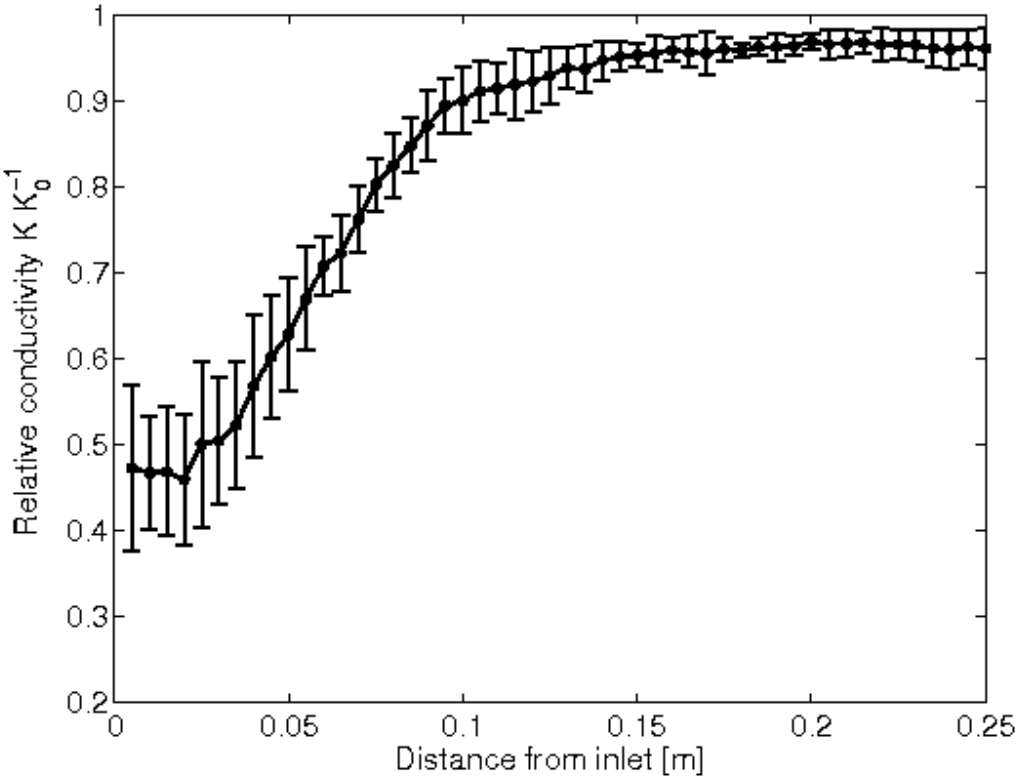

Figure 19. Spatial profile of the hydraulic conductivity along the length of the column. For each cross-section, the mean value and the standard deviation are reported. Initial biomass distribution is log-normal, spatially correlated.